Redox Biology 77 (2024) 103391

Contents lists available at ScienceDirect

Redox Biology

journal homepage: www.elsevier.com/locate/redox

Methionine oxidation of actin cytoskeleton attenuates traumatic memory retention via reactivating dendritic spine morphogenesis

Cun-Dong Huang [a], Yu Shi [a], Fang Wang [a,b,c,d,***], Peng-Fei Wu [a,b,c,d,**], Jian-Guo Chen [a,b,c,d,*]

[a] Department of Pharmacology, School of Basic Medicine, Tongji Medical College and State Key Laboratory for Diagnosis and Treatment of Severe Zoonotic Infectious Diseases, Huazhong University of Science and Technology, Wuhan, Hubei, 430030, China
[b] The Key Laboratory for Drug Target Researches and Pharmacodynamic Evaluation of Hubei Province, Wuhan, Hubei, 430030, China
[c] The Research Center for Depression, Tongji Medical College, Huazhong University of Science and Technology, Wuhan, Hubei, 430030, China
[d] Hubei Shizhen Laboratory, Wuhan, Hubei, 430030, China

ARTICLE INFO

Keywords:
Cued fear conditioning
Actin cytoskeleton
Dendritic spine
Basolateral amygdala
Molecule interacting with CasL 1

ABSTRACT

Post-traumatic stress disorder (PTSD) is characterized by hypermnesia of the trauma and a persistent fear response. The molecular mechanisms underlying the retention of traumatic memories remain largely unknown, which hinders the development of more effective treatments. Utilizing auditory fear conditioning, we demonstrate that a redox-dependent dynamic pathway for dendritic spine morphogenesis in the basolateral amygdala (BLA) is crucial for traumatic memory retention. Exposure to a fear-induced event markedly increased the reduction of oxidized filamentous actin (F-actin) and decreased the expression of the molecule interacting with CasL 1 (MICAL1), a methionine-oxidizing enzyme that directly oxidizes and depolymerizes F-actin, leading to cytoskeletal dynamic abnormalities in the BLA, which impairs dendritic spine morphogenesis and contributes to the persistence of fearful memories. Following fear conditioning, overexpression of MICAL1 in the BLA inhibited freezing behavior during fear memory retrieval via reactivating cytokinesis, whereas overexpression of methionine sulfoxide reductase B 1, a key enzyme that reduces oxidized F-actin monomer, increased freezing behavior during retrieval. Notably, intra-BLA injection of semaphorin 3A, an endogenous activator of MICAL1, rapidly disrupted fear memory within a short time window after conditioning. Collectively, our results indicate that redox modulation of actin cytoskeleton in the BLA is functionally linked to fear memory retention and PTSD-like memory.

1. Introduction

Post-traumatic stress disorder (PTSD) is commonly understood as a memory-based disorder characterized by the co-existence of an increased and persistent traumatic memory. Traumatic memory can be inhibited through extinction, an active learning process that involves repeated exposure to a conditioned stimulus (CS) in the absence of the aversive unconditioned stimulus (US). This process allows for the updating of existing memories with new information, without erasing the original aversive memories [1,2]. Given that PTSD is linked the persistence of vivid and distressing intrusive memories associated with trauma-related fear, suppressing the later retrieval of these traumatic memories would be a promising avenue for treatment of PTSD.

Dendritic spines, which are small protrusions on the dendrites of most excitatory synapses, are dynamic structures that play a crucial role in synaptic plasticity. Numerous studies have demonstrated that auditory fear conditioning, a well-validated paradigm for assessing fear behaviors relevant to traumatic memories, induces long-lasting alterations in dendritic spine and less plastic changes in emotion-associated brain regions, such as BLA, which comprises of the lateral amygdala and the basal amygdala nuclei. These brain regions are closely linked to the deficits in fear memory retention and extinction [3-5]. However, the mechanisms underlying the enduring dendritic spine alterations associated with aversive fear stimuli remain poorly understood.

* Corresponding author. 13 Hangkong Road, Qiaokou District, Wuhan, Hubei, 430030, China.
** Corresponding author. 13 Hangkong Road, Qiaokou District, Wuhan, Hubei, 430030, China.
*** Corresponding author. 13 Hangkong Road, Qiaokou District, Wuhan, Hubei, 430030, China.
E-mail addresses: wangfangtj0322@163.com (F. Wang), wupengfeitjmu@hust.edu.cn (P.-F. Wu), chenj@mails.tjmu.edu.cn (J.-G. Chen).

https://doi.org/10.1016/j.redox.2024.103391
Received 29 July 2024; Received in revised form 29 September 2024; Accepted 8 October 2024
Available online 9 October 2024

Dendritic spines are dynamic structures governed by the assembly and disassembly of F-actin cytoskeletal components. The assembly of actin is driven by its polymerization into F-actin, followed by cross-linking of actin-binding proteins (ABPs) that form stable network structures. Conversely, actin disassembly is initiated by the oxidation of methionine residues 44 and 47 to methionine R-sulfoxide (R-MetO) via molecules interacting with CasL (MICALs), which are recognized as a most prominent F-actin disassembly enzyme. This family comprises three vertebrate members (MICAL1, MICAL2 and MICAL3) and one invertebrate member, Mical [6-8]. Among these, MICAL1 is the most extensively studied and is essential for numerous physiological functions [9-11], while MICAL2 predominantly influences nuclear actin [12], and MICAL3 is notably expressed in breast cancer stem-like cells [13]. MICALs facilitate the depolymerization of the barbed ends of actin filaments, leading to the destabilization of F-actin and subsequent remodeling of the cytoskeleton, a process that is essential for cytokinesis [14-16]. The actin modification induced by MICALs can be selectively counteracted by a family of stereospecific methionine sulfoxide reductase enzymes known as methionine sulfoxide reductase B (MsrB) [17]. Furthermore, alterations in the actin cytoskeleton within the BLA are tightly related to the formation of aversive memories [18-20]. Despite the enormous interest in actin-regulatory proteins and their roles in memory processing, the involvement of redox-dependent F-actin dynamics in fear memory retention and extinction remains inadequately understood. Herein, we demonstrated that deficits in the redox cycle of F-actin underlined the retention of fear stimulus-associated spine alterations. Specifically, F-actin oxidation mediated by MICAL1 actively remodeled the cytoskeleton and dendritic spine structure in the BLA, thereby highlighting the capacity of redox events to disrupt fear memory retention and facilitate fear extinction.

2. Materials and methods

2.1. Animals

Seven-week-old male C57BL/6J mice (20-22 g) were purchased from Hunan SJA Laboratory Animal (Changsha, Hunan, China). All mice were housed in clear plastic cages with four individuals per cage, in a temperature (22-24°C) -and humidity (50-60%) -controlled room. The animal room was maintained on a 12 h light/dark cycle, with food and drinking water available ad libitum.

2.2. Agents

Corticosterone (CORT) was purchased from MCE (HY-B1618, New Jersey, USA), and was diluted to a concentration of 5 mg/kg in drinking water for a duration of 2 consecutive weeks. Recombinant mouse semaphorin (SEMA) 3A was obtained from R&D Systems (5926-S3-025/CF, Minnesota State, USA), diluted in phosphate-buffered saline (PBS) to a concentration of 100 μg/ml, and delivered into the BLA though an intracranial cannula at a volume of 1 μl.

2.3. Stereotactic surgeries

The stereotaxic surgery procedure was performed as previously reported in our lab [21]. Eight to ten-week-old male mice were anesthetized using isoflurane and fixed in a stereotactic frame. Following hair shaving, a small incision was made in the scalp to expose the top of the skull, which was leveled by placing lambda and bregma in the same horizontal plane. LV-transferred vectors were constructed to contain GV640, which encodes the coding sequences of MICAL1 (CMV-MCS-3FLAG-EF1-ZsGreen1-T2A-puromycin) for overexpression of MICAL1, with a final titer of 1.0×10^9 TU (transduction units)/ml. LV-transferred vectors containing GV513 were constructed to encode the coding sequences of MsrB1 (Ubi-MCS-CBh-gcGFP-IRES-puromycin) for overexpression of MsrB1, with a final titer of 1.0×10^9 TU/ml. To knock down MICAL1, an LV harboring shRNA sequence (5′-GTCCAAGCACCACAAGTTCCT-3′) was used (U6-MCS-Ubi-EGFP), with a final titer of 7.0×10^8 TU/ml. LV harboring shRNA sequence (5′-GCTATGAGCTGTTCTCCAGTC-3′) targeting MsrB1 gene was utilized to knockdown MsrB1 (hU6-MCS-CMV-EGFP), with a final titer of 5.0×10^8 TU/ml. All viruses were purchased from GeneChem Company (Shanghai, China). The stereotaxic coordinates for BLA (anteroposterior (AP): -1.70 mm, mediolateral (ML): ±3.40 mm, dorsoventral (DV): -4.00 to -4.20 mm) were taken relative to the bregma, and a volume of 600 nl of concentrated virus solution was injected bilaterally into the BLA at a slow rate of 50 nl/min using a microsyringe pump (Word Precision Instruments, Sarasota, FL, USA). The needle was withdrawn 5 min post-infusion, and the skin was subsequently closed using medical sutures. For cannula implantation, bilateral stainless-steel guide cannula was inserted into the BLA at the following coordinates (relative to bregma): AP: -1.40 mm, ML: ±3.40 mm, DV: -3.50 mm. Following the implantation, the cannula was fixed by applying dental adhesive to the surface of mouse skull around cannula base. All mice were allowed to recover on a heating pad until fully awake. For drug injection, mice were anesthetized with 1.4% isoflurane in a gas mixture comprising 70% nitrous oxide and 30% oxygen, and drugs were injected into the BLA in a volume of 1 μl via the cannula using the microsyringe pump, and the cannula positions were histologically confirmed.

2.4. Cell culture

The HT-22 cell line (31st generation) were purchased from Jennio biotechnology company (JNO-749, Guangzhou, China), and were cultured in six-well plates with Dulbcco's Modified Eagle Medium (DMEM) supplemented with 10% fetal bovine serum, 100 U/ml of penicillin and streptomycin at 37°C in a 5% CO_2 incubator. The cells were incubated with CORT (1 μM) for 24 h prior to harvesting. Subsequently, protein samples were measured using western blotting.

2.5. Cued fear conditioning and extinction procedure

Cued fear conditioning and extinction were conducted as our previous reports with slight modifications [22,23]. The procedures took place in conditioning chambers ($32 \times 26 \times 30$ cm^3) situated in two distinct contexts: context A and context B. Context A, the conditioning context, was characterized by an original conditioning chamber with transparent acrylic walls and a bare stainless-steel grid floor. In contrast, context B, designated as extinction context, was modified by covering the stainless-steel grid floor with a black acrylic platform and adorning the chamber walls with black and white stickers. For the cued fear conditioning, mice were placed in a shock chamber (Coulbourn Instruments), which was cleaned with 70% ethanol prior to each experiment. Following a 2 min habituation period in context A, mice underwent fear conditioning involving 5 tone-shock pairings, where a 30 s (5 kHz, 80 dB) tone (CS) co-terminated with a 2 s (0.8 mA) foot shock (US). Control mice were exposed to 5 CS-only presentations without the US. Intertrial intervals (ITIs) between each tone-shock pairing were set at 30 s. For fear memory retrieval, after a 2 min habituation period (Pre-CS), mice were presented with 2 CS-only presentations in the conditioning context, each consisting of a 30 s tone followed by a 30 s interval. Extinction learning occurred over 2 consecutive days (Ext 1 and Ext 2) in context B, consisting of 12 presentations of CS (with ITIs of 30 s) without the US. For extinction, conditioned mice that exposed to context B for 12 min over the 2 days without any CS or US (no extinction group) were defined as controls. The extinguished fear test was performed 24 h after the final extinction learning session in context B. Freezing behavior was monitored using an infrared beam detection system integrated within the fear conditioning apparatus, and video recordings were subsequently transferred to a computer equipped with an analysis program (Kinder Scientific, California, USA), where the freezing behavior was automatically quantified

using the MotorMonitor Π software.

2.6. Open field and elevated plus maze

Open field test was conducted in an operating box (42 cm wide by 42 cm high by 42 cm deep). Each mouse was placed in the center quarter, and a video camera was used to record movements for a duration of 10 min. For the elevated plus maze test, the maze consisted of two opposing open arms (30 cm × 5 cm × 0.5 cm) and two closed arms (30 cm × 5 cm × 15 cm) extending from a central platform (5 cm × 5 cm) and was elevated 40 cm above the ground. Mice was placed on the center platform of the crossed maze, and allowed to explore freely for 5 min. The time spent in open arms were manually scored by the ANY-maze tracking system 5.3 (Stoelting Co., Wood Dale, IL, USA).

2.7. Western blotting analysis

Western blotting was performed as previously described [24]. Briefly, cell or tissue samples were homogenized in ice-cold radioimmunoprecipitation lysis buffer containing protease and phosphatase inhibitors (50 mM Tris-HCl pH 7.5, 150 mM NaCl, 0.1% sodium dodecyl sulfate, 1% Triton X-100, 1% sodium deoxycholate). The samples were lysed on ice for 30 min and subsequently centrifuged at 12,000 *g* for 20 min at 4°C. Protein concentration was quantified using the bicinchoninic acid assay protein assay kit (P0012, Beyotime Biotechnology, Shanghai, China). All protein samples were boiled with loading buffer in a mini-mental bath at 95°C for 10 min. A total of 30 μg of each protein sample was separated by 10% or 12% sodium dodecyl sulfate-polyacrylamide gel electrophoresis and then transferred to nitrocellulose membranes at 15 V for 45 min. The membranes were blocked with 5% bovine serum albumin (BSA, Merck Millipore, Billerica, MA, USA) in Tris-buffered saline containing 0.1% Tween-20 (TBST) at room temperature for 1 h, followed by overnight incubation at 4°C with various primary antibodies: anti-MICAL1 (1:1,000, 14818-1-AP, Proteintech Group Lnc., Chicago, USA), anti-MICAL2 (1:1,000, AP52693PU-N, OriGene Technologies Lnc., Maryland, USA), anti-MsrA (1:1,000, ab16803, Abcam, Cambridge, UK), anti-MsrB1 (1:1,000, PA5-77009, Thermo Fisher Scientific, Massachusetts, USA), anti--β-actin (1:2,000, sc-47778, Santa Cruz Biotechnology, California, USA), anti-GAPDH (Glyceraldehyde-3-phosphate dehydrogenase) (1:2,000, ab128915, Abcam, Cambridge, UK). After washing the membranes 3 times with TBST, secondary antibodies (1:10,000, LI-COR, Lincoln, USA) were applied and incubated for an additional hour at room temperature. Following another wash, the antibody-reactive bands were visualized and analyzed using the LI-COR imaging system (Lincoln, USA).

2.8. Ratio of F-actin to G-actin assay

The ratio of F-actin to G-actin was quantified using a G-actin/F-actin *in vivo* assay kit (BK037, Cytoskeleton, lnc., Denver, USA) according to the manufacturer's instructions [25]. Briefly, the BLA tissue was freshly isolated and snap-frozen in liquid nitrogen. Prior to the assay, a specialized lysate was prepared by adding 10 μl of a 100 × protease inhibitor cocktail and 10 μl of a 100 nM ATP stock solution to 1000 μl of F-actin stabilization buffer, which was then mixed thoroughly and incubated at 37°C for 30 min. Subsequently, 10 μl of lysate per mg of tissue was added immediately for homogenization, followed by a 10 min incubation at 37°C. Each lysate was centrifuged at 350 *g* for 5 min, and the supernatant was transferred into a pre-warmed (37°C) ultracentrifuge tube for ultracentrifuge (Beckman coulter lnc., USA) at 100,000×*g*, 37°C for 1 h to pellet F-actin, leaving G-actin in the supernatant. Each pellet was further resuspended in 100 μl of F-actin depolymerization buffer and incubated on ice for 1 h. All samples were diluted with 25 μl of 5 × sodium dodecyl sulfate sample buffer, mixed thoroughly, and heat-denatured at 95°C for 10 min. F-actin and G-actin fractions were separated using 10% sodium dodecyl sulfate-polyacrylamide gels, and western blotting was performed to analyze the levels of F-actin and G-actin using a mouse anti-Actin (1:1000) antibody included in the kit.

2.9. Methionine oxidation of F-actin assay

The tissue of the BLA was gently lysed in immunoprecipitation buffer NP-40 (P0013F, Beyotime Biotechnology, Shanghai, China), which contained a protease inhibitor cocktail and phenylmethanesulfonyl fluoride (PMSF) (ST507, Beyotime Biotechnology, Shanghai, China), for 30 min on ice. The lysate was then centrifuged at 12,000 *g* for 20 min at 4°C. Each sample's supernatant (500 μg) was immunoprecipitated with mouse anti-F-actin (1:50, ab205, Abcam, USA) antibody overnight at 4°C. Subsequently, 20 μl of protein A/G plus agarose (sc-2003, Santa Cruz Biotechnology, California, USA) was added to the supernatant and incubated for 4 h at room temperature, followed by centrifuging at 4000 *g* for 5 min at 4°C. Each immunoprecipitants were washed 3 times for 10 min with NP-40 and centrifuged at 450 *g* for 3 min. The immunoprecipitants were then added to 20 μl of 2 × sodium dodecyl sulfate loading buffer and heated at 95°C for 10 min. The level of F-actin methionine oxidation was detected by western blotting analysis using rabbit anti-MetO antibody (600,160, 1:200, Cayman Chemical Co., Michigan, USA).

2.10. Biochemical analysis

The concentration of hydrogen peroxide (H_2O_2) in the BLA was evaluated using a commercially available kit (A064-1-1, Nanjing Jiancheng Bioengineering Institute, China). In this process, H_2O_2 reacted with molybdenic acid to form a complex, which was subsequently quantified at 405 nm using a multimode plate reader (infinite M200 PRO, Tecan, Switzerland). The H_2O_2 content was then calculated based on these measurements. Additionally, the concentration of malondialdehyde (MDA) in the BLA homogenate was determined using another commercially available kit (A003-1-2, Nanjing Jiancheng Bioengineering Institute, China), which is based on thiobarbituric acid (TBA) reactivity. In brief, trichloroacetic acid was mixed with the homogenate, followed by centrifugation to obtain a supernatant. TBA was then added to the supernatant, and the intensity of the developed red color from the reaction was measured at 532 nm using a multimode plate reader.

2.11. Phalloidin staining

Mice were anesthetized using pentobarbitone sodium and subsequently underwent transcardial perfusion with saline, followed by 4% paraformaldehyde. Isolated brain tissues were fixed in 4% paraformaldehyde overnight and then immersed in 15% and 30% sucrose at 4°C overnight, respectively. The brain tissues that sank to the bottom of the container were embedded in optimal cutting temperature compound and immediately frozen in a -80°C freezer. Serial sections were obtained using a freezing microtome (CM1900, Leica Biosystems, Wetzlar, Germany) at -20°C. Phalloidin staining were performed as previous report, with some modifications [26]. The slices (30 μm) were permeabilized with 0.3% Triton X-100 in PBS for 1 h at room temperature, and non-specific binding sites were blocked using a blocking solution (0.3% Triton X-100 and 5% BSA in PBS) for 1 h at room temperature. Subsequently, the slices were labeled with Actin-stain™ 555 phalloidin (1:200, Cytoskeleton lnc., Denver, USA) for 1 h at room temperature in the dark, followed by 3 times washes with PBS. The nuclei were stained with 4′, 6-diamidino-2-phenylindole in PBS for 10 min at room temperature. All images were obtained using an Olympus confocal microscope (FV1000, Ishikawa, Japan) equipped with a 60 × oil-immersion objective lens, which allowed for an electronic zoom factor of up to 2.0. All the microscope settings were kept consistent in each experiment, maintaining a light transmissivity of 25% at a wavelength of 594 nm. XY scanning was employed to capture a single confocal image from a horizontal plane, as determined by the clarity of the live image displayed on

the screen during rapid XY scanning. For the analysis of F-actin fluorescence, images were imported into Imaris software (Bitplane, Zurich, Switzerland). The fluorescence intensity of F-actin was identified using the threshold function with the Imaris software with an intensity value of 200. The software automatically scored the fluorescence intensity based on the defined profiles.

2.12. Dendritic spines staining

Dendritic spines were quantified following established protocols with some modifications [27]. Specifically, the BLA were infected with lentivirus containing green fluorescent protein (5′-TTCTCCGAACGTGTCACGT-3′, LV-GFP) to enable visualization of the neurons, and the mice underwent various treatments after two weeks. At 24 h after cued fear memory or extinction retrieval test, mice were deeply anesthetized with sodium pentobarbital (45 mg/kg, administered via intraperitoneal injection) and subsequently perfused intracardially with 0.9% saline, followed by 4% paraformaldehyde in phosphate-buffered saline (0.1 M, pH 7.4). The brains were fixed in 4% paraformaldehyde solution for 24 h and then gradient dehydration in phosphate-buffered saline containing 15% and 30% sucrose for one day each. Serial coronal slices (50 μm thick) containing the BLA were obtained using a freezing microtome. For the analysis of dendritic spines, sections were placed onto microscope slides, treated with 10 μl of phosphate-buffered saline containing 50% glycerol, and gently covered with a coverslip. Confocal Z-stack images were captured using a confocal microscope equipped with a 100 × oil-immersion objective lens and an additional electronic zoom factor of up to 2.0. Imaris software was employed to measure the number and length of dendritic spines from 3D reconstruction. The number and density of spines were normalized per 10 μm of dendritic length and spine types were classified as mushroom, stubby or long/thin based on specific parameters.

2.13. Statistical analysis

Mice in all experiments were randomly assigned to different groups. Sample size was set according to those used in similar studies from our laboratory [21]. Data analysis was performed using GraphPad Prism 8.3 (GraphPad Prism, California, USA). The Shapiro–Wilk test or the D'Agostino and Pearson test was performed to assess the normality of samples. The F-test or Brown-Forsythe or Bartlett's test was used to evaluate equality of standard deviations. The differences between two groups were assessed using Student's t-test or Mann Whitney tests. One-way ANOVA was applied for comparisons involving more than two groups, and two-way ANOVA with Bonferroni correction was implemented for comparisons across different conditions. All data were presented as mean ± SEM. $p < 0.05$ was considered statistically significant.

3. Results

3.1. Fear conditioning induces reversible changes in dendritic spine morphology and cytoskeleton dynamics in BLA

The BLA serves as a central hub for salience networks that underpin emotional experience and plays a critical role in the formation of long-term fear memory [28,29]. To investigate the effects of cued fear conditioning and extinction on the morphology of dendritic spines in the BLA, mice were bilaterally injected with lentivirus containing green fluorescent protein (LV-GFP) for a duration of 2 weeks. Subsequently, the mice underwent training in a cued fear conditioning paradigm, wherein a tone (CS) was paired with an aversive foot shock (US) following a 5 min habituation period to the CS in the conditioning context (Context A) (Fig. 1A). Compared to the control mice, conditioned mice displayed comparable freezing behavior prior to CS presentation, but exhibited a significant increase in freezing response during successive CS presentations throughout the memory acquisition phase (Fig. S1A). On the following day, all mice were placed in the conditioning context for fear memory retrieval. Notably, conditioned mice demonstrated an elevated freezing behavior even in the absence of CS presentation, while CS presentations elicited a markedly higher freezing response compared to the control mice (Fig. S1B). Furthermore, the conditioned mice exhibited similar levels of spontaneous activity, anxiety-like and social behaviors compared to the control mice (Fig. S1C–E). Subsequently, we observed an increase in the density of dendritic spines in the BLA of the conditioned mice (Fig. 1B and C), which were consistent with previous study [30]. The spines were further classified into three morphological subtypes: stubby, mushroom and long/thin shapes. Our analysis revealed that the densities of all spine types were significantly increased in the BLA of the conditioned mice (Fig. 1D-F). Actin is the principal cytoskeletal protein, existing in two forms: globular actin (G-actin) and F-actin, which is polymerized from G-actin. Given that alterations in the morphology of dendritic spines can be influenced by the dynamics between G-actin and F-actin [31,32], we asked whether fear-induced changes in dendritic spines would correlate with actin dynamics in the BLA. Our findings revealed that, compared to the control mice, the ratio of F-actin to G-actin was significantly increased in the BLA of the conditioned mice (Fig. 1G).

Next, we examined the impact of fear extinction learning on dendritic spines in the BLA. Mice were subjected to cued fear conditioning in context A, and 24 h later, the equivalent fear acquisition mice were trained by an extinction learning in context B (Fig. S1F), which differed from context A to minimize the effects of contextual memory, over 2 consecutive days (Ext 1 and Ext 2) by presenting 12 CSs on each day (Fig. 1A). The conditioned mice that were exposed only to context B, without the presentation of the CS, served as the no extinction group. Extinction retrieval was conducted 24 h following the final extinction session in context B, during which the mice extinguished their fear responses compared to the no extinction group (Fig. S1G). Post-retrieval, we analyzed the dendritic spines in the BLA 24 h later. The total density of dendritic spines in the extinction group was significantly lower than that of the no extinction group (Fig. 1H and I), with a notable decrease in the density of mushroom-shaped spine (Fig. 1J), while the dendritic of stubby- and long/thin-shaped spines remained unchanged (Fig. 1K and L). Additionally, the ratio of F-actin to G-actin in the BLA was decreased following extinction (Fig. 1M). To visualize F-actin, we stained F-actin with phalloidin, which selectively binds to the polymerized form of actin. In the no extinction group, we observed a marked increase in F-actin fluorescence compared to the control group, which was subsequently reversed by extinction (Fig. 1N). Collectively, these findings indicate that extinction may partially turnover the ratio between F-actin and G-actin, potentially reversing the fear conditioning-induced increase in dendritic spines.

3.2. Fear conditioning decreases the oxidation of actin methionine residues in BLA

The turnover between F-actin and G-actin is regulated by the disassembly of actin, with MICALs being the most prominent enzymes responsible for F-actin disassembly. MICALs directly depolymerize F-actin within a specific oxidation of methionine residues to R-MetO [6,8]. Then, we examined the effects of cued fear conditioning on the oxidation of actin methionine residues and its associated redox parameters. Following cued fear conditioning, the BLA were collected at 1 h, 2 h, 24 h and 2 w to measure the expression levels of MICALs and methionine sulfoxide reductase enzymes (Fig. 2A). It was found that the expression of MICAL1 in the BLA was decreased at 2 h after cued fear conditioning (Fig. 2B), while levels of methionine sulfoxide reductase A (MsrA) and MsrB1, two key methionine sulfoxide reductases, were elevated at 1 h or 2 h post-conditioning, respectively (Fig. 2C and D). At 24 h post-conditioning, MICAL1 expression remained reduced in the BLA (Fig. 2E). Considering MICAL2 is predominantly localized in nucleus and is known to regulate nuclear gene transcription [12], which may

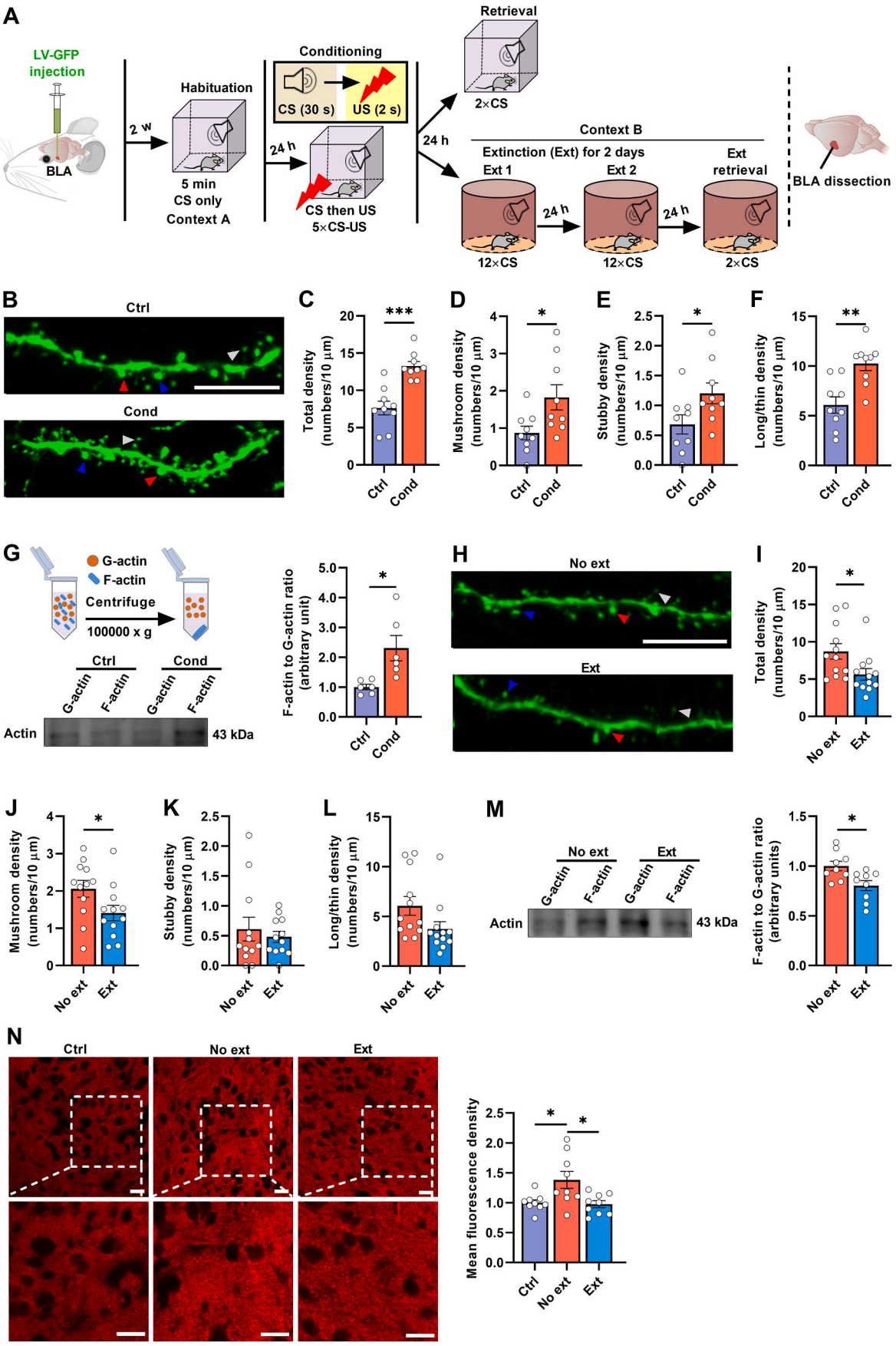

(caption on next page)

Fig. 1. Fear conditioning induces reversible changes in dendritic spine morphology and cytoskeleton dynamic in BLA. (A) Schematic of the experimental design. (B) Representative images of dendritic spines in the BLA from control and conditioned mice. Scale bars: 10 μm. Blue arrows indicate mushroom-shaped spines, red arrows indicate stubby-shaped spines, and white arrows indicate long/thin-shaped spines. (C-F) Fear conditioning resulted in an increased density of (C) total, (D) mushroom-, (E) stubby- and (F) long/thin-shaped spines in the BLA of conditioned mice (n = 9 neurons from 3 mice per group). (G) The ratio of F-actin to G-actin in the BLA of conditioned mice was significantly elevated (n = 6 mice per group). (H) Representative images of dendritic spines in the BLA of no extinction and extinction mice. Blue arrows: mushroom-shaped spines; Red arrows: stubby-shaped spines; White arrows: long/thin-shaped spines. Scale bars: 10 μm. (I-L) Extinction learning reversed the increases in density of (I) total and (J) mushroom-shaped spines in the BLA, but not (K) stubby- or (L) long/thin-shaped spines (n = 12 neurons from 4 mice per group). (M) Extinction learning decreased the ratio of F-actin to G-actin in the BLA (n = 9 mice per group). (N) Confocal images of F-actin staining using phalloidin in the BLA slices of control, no extinction and extinction mice. Scale bars: 20 μm. Extinction learning resulted in a decreased fluorescence density of F-actin in the BLA (n = 9 slices from 3 mice per group). Ctrl: control; Cond: conditioned; Ext: Extinction; No ext: no extinction. Two-tailed, unpaired *t* tests (C, D, E, F, J, L, M); unpaired *t*-test with Welch's correction (G); two-tailed, Mann Whitney tests (I, K); one-way ANOVA with Tukey's multiple comparisons tests (N). $^{*}p < 0.05$, $^{**}p < 0.01$ and $^{***}p < 0.001$. Data are presented as the mean ± SEM. (For interpretation of the references to color in this figure legend, the reader is referred to the Web version of this article.)

play a role in the enduring synaptic modifications during the late phase of learning, we evaluated MICAL2 at 24 h after fear conditioning; however, we observed no significant change in its expression levels (Fig. 2F). Concurrently, MsrB1 levels increased (Fig. 2G), while MsrA levels did not change (Fig. 2H), indicating a disruption in the actin methionine redox cycle. Importantly, there was no significant difference in MICAL1 expression in other brain regions associated with fear, including central amygdala (Fig. S2A), medial prefrontal cortex (Fig. S2B), anterior cingulate cortex (Fig. S2C), dorsal and ventral hippocampus (Fig. S2D and E) between control and conditioned mice. Notably, even two weeks after cued fear conditioning, a persistent decrease in MICAL1 levels, but not in MsrB1 levels, was observed in the BLA of conditioned mice (Fig. 2I and J), suggesting a sustained disruption in the actin methionine redox cycle occurs in the BLA following trauma.

To further ascertain the effect of fear conditioning on the oxidation of actin methionine residues, the immunoprecipitation was applied to isolate F-actin, subsequently examining methionine oxidation using anti-MetO antibody (Fig. 2K). Our findings indicate that 24 h after fear conditioning, the level of F-actin MetO significantly decreased (Fig. 2L), while the total level of MetO remained unchanged in the BLA (Fig. 2M), suggesting that redox-dependent F-actin dynamics are altered by fear conditioning, which may contribute to the observed behavioral outcomes.

3.3. MICAL1-mediated oxidation of actin in BLA disrupts cued fear memory

We hypothesized that deficits in redox-dependent actin filament disassembly in the BLA may underlie the retention of fear memory. To investigate this, we injected LV-GFP containing the coding sequences of MICAL1 (LV-MICAL1) into the bilateral BLA of conditioned mice to overexpress MICAL1, subsequently examining its effects on the fear memory retention (Fig. 3A). LV-GFP was utilized as the control. First, the efficacy of virus infection was confirmed by the appearance of green fluorescence (Fig. 3B) and western blotting assay (Fig. S3A). Second, compared to LV-GFP group, the oxidation of F-actin methionine residues (Fig. 3C), but not the total MetO level (Fig. 3D), was increased in the BLA from LV-MICAL1 group. Although all conditioned mice displayed equivalent freezing response during the CS-US association learning prior to the injection of LV-GFP or LV-MICAL1 into the BLA (Fig. 3E), only the LV-MICAL1 group showed a reduction in freezing behavior on retrieval (Fig. 3F), without affecting spontaneous activity or anxiety-like behavior (Fig. S3B and C). Furthermore, we detected the levels of H_2O_2 and MDA in the BLA, as it has been demonstrated that MICALs may release the diffusible oxidant H_2O_2 in conjunction with their catalytic activity. No significant differences in H_2O_2 and MDA content were observed between LV-GFP and LV-MICAL1 groups (Fig. 3G and H), suggesting that the behavioral consequence may be not due to the non-enzymatic oxidation associated with MICAL1.

To further strengthen the functional relationship between redox-dependent F-actin disassembly and fear memory retention, the expression of MsrB1 that directly reduced MICAL-oxidized actin and restored its polymerization properties was knock downed though bilateral injection of LV that contains the short hairpin RNA (shRNA) sequences targeting MsrB1 (LV-shMsrB1) into BLA after fear conditioning. LV-scramble was served as the control. Virus infection at BLA was confirmed by the green fluorescence and western blotting assay (Fig. 3I, Fig. S3D). Subsequently, mice exhibiting equivalent freezing response were selected for injection with LV-scramble or LV-shMsrB1 into the bilateral BLA (Fig. 3J). Two weeks post-injection, the LV-shMsrB1 group showed a lower freezing behavior on retrieval compared to the LV-scramble group (Fig. 3K), without affecting spontaneous locomotion or anxiety-like behavior in an open field and elevated plus maze test between groups (Fig. S3E and F). Collectively, these results suggest that increased methionine oxidation of actin in the BLA may disrupt cued fear memory retention.

3.4. Overexpression of MICAL1 in BLA facilitates the extinction of cued fear memory

The BLA is critical for fear attenuation induced by exposure therapy-like extinction protocols [33,34]. We further examined the role of actin oxidation status on the process of fear extinction. To test this possibility, a cohort of 35 mice underwent cued fear conditioning, from which 24 conditioned mice were selected for extinction learning over the following 2 days (Fig. 4A), and conditioned mice that also exposed to extinction context but without any CS or US (no extinction group) were served as the controls. Following the final extinction learning, all mice underwent extinction memory retrieval, the extinction mice that exhibited a freezing percentage below 20% (16.18 ± 2.25%) were categorized as extinction success (Ext-success) mice. In contrast, those mice underwent extinction learning that displayed a freezing percentage exceedingly twice that of the Ext-success mice were defined as extinction failure (Ext-failure) mice (33.29 ± 3.08%) (Fig. 4B). The BLA was obtained immediately after retrieval. Compared to the Ext-failure or no extinction group, the expression of MICAL1, rather than MsrB1, was found to be elevated in the BLA of Ext-success mice (Fig. 4C and D), indicating that MICAL1 may be involved in extinguished fear memory.

To explore this possibility, mice with comparable fear acquisition were injected with LV-MICAL1 into the bilateral BLA to overexpress MICAL1 gene 24 h after fear conditioning (Fig. 4E and F). LV-GFP was severed as the control. After two weeks, the mice underwent an extinction learning paradigm, revealing that mice overexpressing MICAL1 in the BLA showed a better performance in extinction learning on day 1 and day 2 (Fig. 4G and H). Notably, LV-MICAL1 group showed a decreased extinguished fear response on extinction retrieval compared to the LV-GFP group (Fig. 4I).

Next, we injected LV-shMICAL1 into the bilateral BLA of mice with equivalent fear acquisition for knockdown of MICAL1 gene 24 h after conditioning. LV-scramble was used as the control. The effectiveness of virus was confirmed by green fluorescence and western blotting assay (Fig. 4J, Fig. S4A). Although both the LV-scramble and LV-shMICAL1 groups exhibited similar freezing response during conditioning

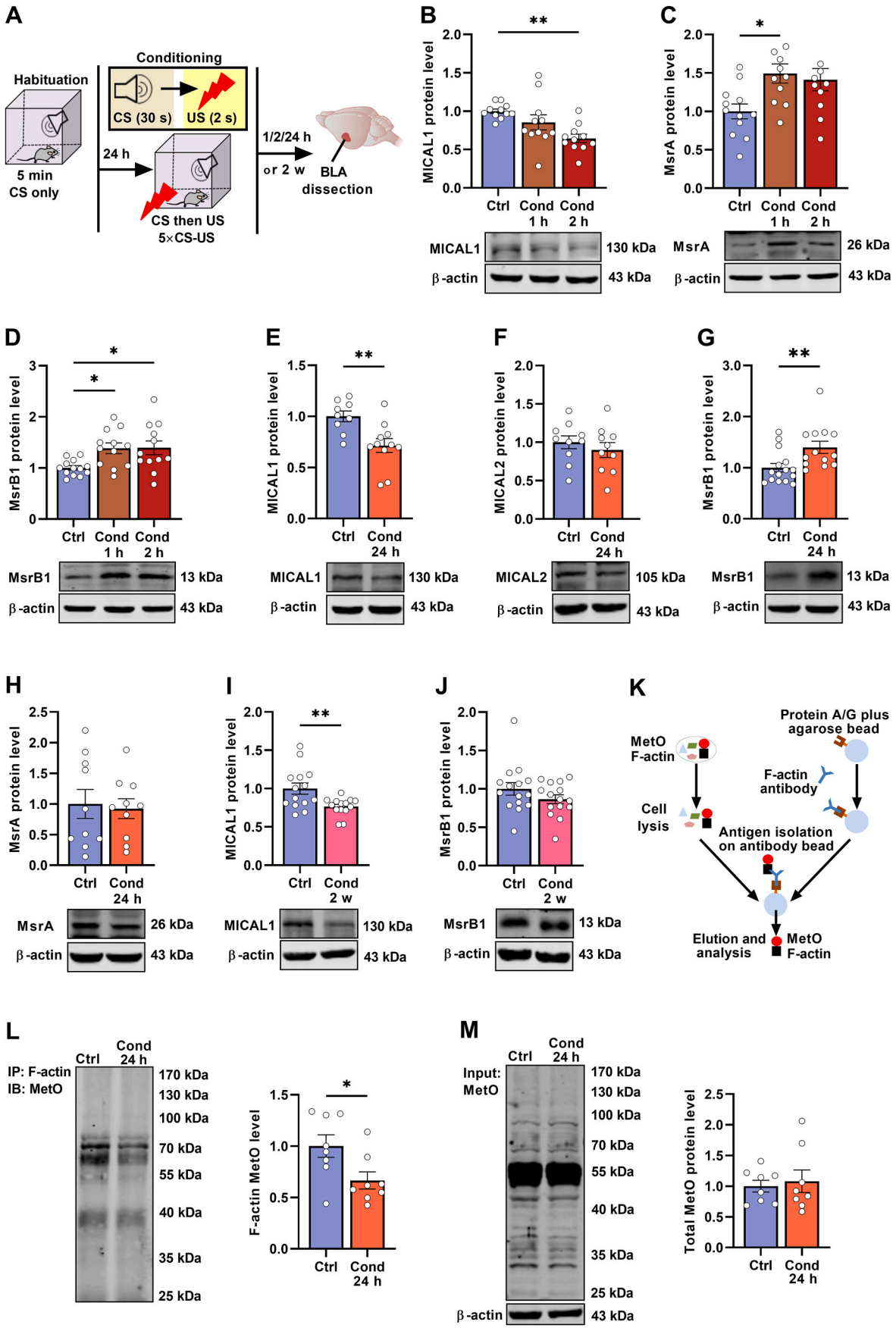

(caption on next page)

Fig. 2. Fear conditioning decreases the oxidation of actin methionine residues in BLA. (A) Schematic of the experimental design. (B) A significant decrease in protein level of MICAL1 in the BLA of conditioned mice was observed at 2 h post-conditioning (n = 11 mice per group). (C, D) An increased protein level of (C) MsrA and (D) MsrB1 in the BLA of conditioned mice at 1 h post-conditioning (n = 11–12 mice per group). (E-F) At 24 h post-conditioning, a decrease in protein level was noted for (E) MICAL1 in the BLA, while (F) MICAL2 level remained unchanged in conditioned mice (n = 9–11 mice per group). (G) An increase in of MsrB1 protein level was detected in the BLA of conditioned mice at 24 h post-conditioning (n = 13–15 mice per group). (H) The protein level of MsrA in the BLA was showed no significant differences between control and conditioned mice at 24 h post-conditioning (n = 10 mice per group). (I-J) At 2 w post-conditioning, there was a notable decrease in the level of (I) MICAL1, while (J) MsrB1 level remained unchanged in the BLA of conditioned mice (n = 14–15 mice per group). (K) Schematic diagram for illustrating the immunoprecipitation of F-actin interaction with MetO. (L) A decrease in the level of F-actin MetO in the BLA of conditioned mice was observed at 24 h post-conditioning (n = 8 mice per group). (M) No obvious difference in the total level of MetO in the BLA was found at 24 h post-conditioning between control and conditioned mice (n = 8 mice per group). Ctrl: control; Cond: conditioned. One-way ANOVA with Tukey's multiple comparisons tests (B, C, D); two-tailed, unpaired *t* tests (E, F, H, J, L, M); two-tailed, Mann Whitney tests (G); two-tailed, unpaired *t*-test with Welch's correction (I); $^{*}p < 0.05$, $^{**}p < 0.01$. Data are presented as the mean ± SEM.

(Fig. 4K), the LV-shMICAL1 group showed an increased freezing response during extinction learning on day 2, but not on day 1 (Fig. 4L and M). Remarkably, the LV-shMICAL1 group showed an elevated extinguished fear response on extinction retrieval compared to the LV-scramble group (Fig. 4N). No obvious difference in spontaneous locomotion was observed between the two groups in the open field test (Fig. S4B–D). Furthermore, we tested the effect of MsrB1 on fear extinction. Similarly, mice with equivalent fear acquisition were selected for injection with LV-scramble or LV-shMsrB1 into the bilateral BLA 24 h after conditioning (Fig. S4E and F), followed by 2 consecutive days of extinction learning 2 weeks later (Fig. S4G and H). However, both groups showed a similar extinguished fear response on extinction retrieval (Fig. S4I). Taken together, these data suggest that MICAL1 in the BLA contributes to extinguish the fear memories.

3.5. Corticosterone-altered MICAL1 expression is involved in the PTSD-like memories

Prolonged periods of stress or chronic exposure to the stress hormone CORT enhances stress-related memories, accompanied by changes of synaptic plasticity in the BLA, which have been involved in the pathophysiology of PTSD [35,36]. We wondered whether MICAL1 would be a candidate stress-related protein that regulated PTSD-like memories such as stress-enhanced fear learning. First, to assess the direct effects of CORT on MICAL1 protein expression, we conducted an experiment in which HT-22 cells were incubated with CORT at a concentration of 1 μM. Following 24 h incubation, we observed a decrease in MICAL1 expression following CORT treatment. (Fig. 5A). Next, we investigated the effects of chronic exposure to CORT on the expression of MICAL1 in BLA *in vivo*. Mice were administered CORT exposure in their drinking water for two weeks. As predicted, CORT exposure resulted in a significant reduction in MICAL1 expression in the BLA (Fig. 5B), while no changes were observed in the expression levels of MsrA and MsrB1 (Fig. 5C and D). We also noted that CORT exposure increased freezing behavior on fear memory retrieval, without affecting fear memory acquisition (Fig. S5A–C). Taken together, these data indicated that MICAL1 may work as a potential candidate for a stress-responsive protein.

Furthermore, we wondered whether the downregulation of MICAL1 was essential to the retention of stress-enhanced fear memory. Mice that exhibited equivalent fear acquisition were injected with either LV-scramble or LV-shMICAL1 into the bilateral BLA 24 h after cued fear conditioning (Fig. 5E and F). Two weeks later, we observed that the LV-shMICAL1 group retained a stable freezing behavior on fear memory retrieval compared to the LV-scramble group (Fig. 5G), indicating that downregulation of MICAL1 expression in the BLA mimics the effects of CORT on enhancing stress-related memories. A similar outcome was observed in MsrB1-overexpressed (LV-MsrB1) mice. LV-GFP was used as the control. It was shown that overexpression of MsrB1 in the BLA (Fig. 5H, Fig. S5D) of mice, which exhibited comparable fear acquisition (Fig. 5I), resulted in an increase in freezing behavior on fear memory retrieval (Fig. 5J), without affecting spontaneous activity and anxiety-like behaviors (Fig. S5E and F). Consequently, we proposed that stress-induced downregulation of MICAL1 conferred to the PTSD-like memory. To address this issue, a new cohort of mice were trained in cued fear conditioning immediately following two weeks of CORT drinking, after which they were injected with either LV-GFP or LV-MICAL1 into the bilateral BLA 24 h after conditioning (Fig. 5K). No significant differences in freezing response were observed in cued fear conditioning in CORT-exposed mice (Fig. 5L). However, two weeks later, the LV-MICAL1 group exhibited a notable reduction in freezing behavior when exposed to the CS on fear memory retrieval (Fig. 5M). Thus, our data provides compelling evidence that MICAL1 may act as a critical mediator of abnormal stress responses following psychological trauma, contributing to the development of PTSD-like memories.

3.6. MICAL1-mediated methionine oxidation of actin cytoskeleton reverses fear conditioning-induced increase in dendritic spines in BLA

Actin polymerization is fundamental to the structural plasticity of dendritic spines, as it facilitates cytoskeleton remodeling, which is essential for the formation of new memories [37,38]. We sought to investigate whether the overexpression of MICAL1 gene would influence both actin cytoskeleton and structural plasticity of the dendritic spines. The equivalent fear acquisition mice were injected with LV-GFP or LV-MICAL1 into the bilateral BLA (Fig. 6A). Two weeks later, both the ratio of F-actin to G-actin and the fluorescent density of F-actin in the BLA were decreased in the LV-MICAL1 group (Fig. 6B and C). We also observed that the densities of total spines in the BLA were decreased in the conditioned MICAL1-overexpressed mice (Fig. 6D and E). Notably, selective overexpression of MICAL1 in the BLA significantly decreased the densities of mushroom- and long/thin-shaped spines of the conditioned mice (Fig. 6F and G), but it exerted no obvious effect on stubby-shaped spines (Fig. 6H).

To further strengthen the role of redox-dependent F-actin disassembly in the structural plasticity of dendritic spines, we took advantage of a new cohort of mice to subject cued fear conditioning, and the comparable fear acquisition mice were injected with LV-scramble or LV-shMsrB1 into the bilateral BLA 24 h after fear conditioning. After two weeks, compared to LV-scramble group, we observed a reduction in the total densities of spines in the BLA of conditioned mice in the LV-shMsrB1 group (Fig. 6I and J). Specifically, the densities of mushroom- and long/thin-shaped spines in the BLA of conditioned mice were significantly decreased in LV-shMsrB1 group (Fig. 6K and L), There was no obvious difference in the densities of stubby-shaped spines in the BLA between LV-scramble and LV-shMsrB1 groups, regardless of whether the mice were in control groups or conditioned groups (Fig. 6M).

In summary, our above observations indicate that the increase in F-actin methionine oxidation by MICAL1 overexpression or MsrB1 gene knockdown orchestrated fear conditioning-induced structural plasticity of dendritic spines in the BLA, which may lead to destabilization of fear memories.

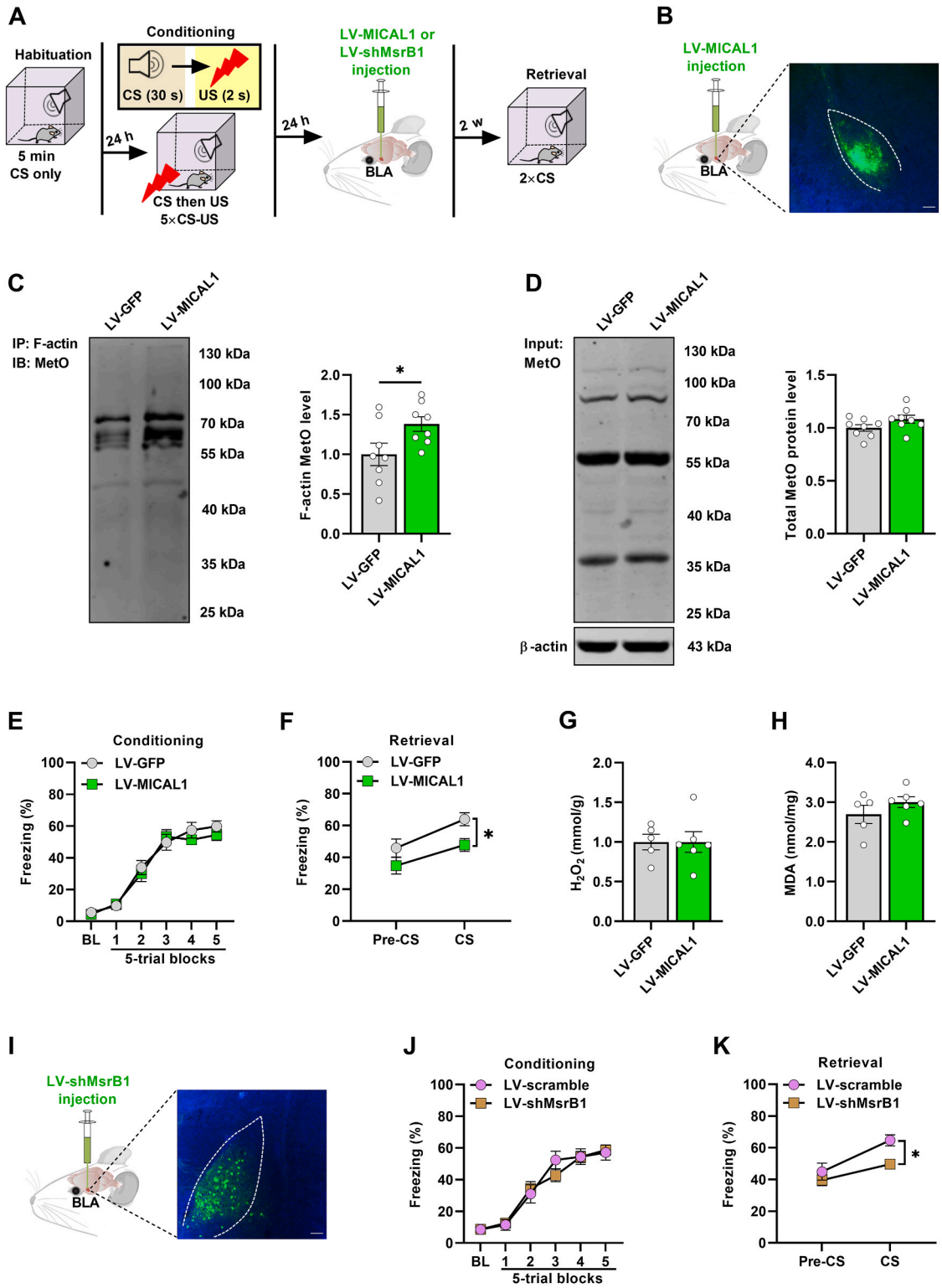

Fig. 3. MICAL1-mediated oxidation of actin in BLA disrupts cued fear memory. (A) Schematic of the experimental design. (B) Schematic representation illustrating the validation of immunohistochemistry for the selective expression of lentivirus constructs in the BLA. Scale bars: 100 μm. (C) The level of F-actin MetO in BLA lysates was significantly increased in the LV-MICAL1 group (n = 8 mice per group). (D) No significant difference in total level of MetO in the BLA was observed between LV-GFP and LV-MICAL1 groups (n = 8 mice per group). (E) The LV-GFP and LV-MICAL1 groups showed equivalent fear acquisition during conditioning (n = 13 mice per group). (F) Overexpression of MICAL1 in the BLA resulted in a decreased freezing behavior on retrieval (n = 19 mice per group). (G, H) The concentrations of (G) H_2O_2 and (H) MDA in the BLA were similar between the LV-GFP and LV-MICAL1 groups (n = 5–6 mice per group). (I) Schematic representation of the immunohistochemistry validation of the restrictive expression of the lentivirus constructs in the BLA. Scale bars: 100 μm. (J) The LV-scramble and LV-shMsrB1 groups exhibited comparable fear acquisition during conditioning (n = 15–16 mice per group). (K) Knockdown of MsrB1 in the BLA resulted in a decreased freezing level on retrieval (n = 15–16 mice per group). Two-tailed, unpaired *t* tests (C, D, G, H); two-way ANOVA with Bonferroni's multiple comparisons post hoc tests (E, F, J, K). $^*p < 0.05$. Data are presented as the mean ± SEM.

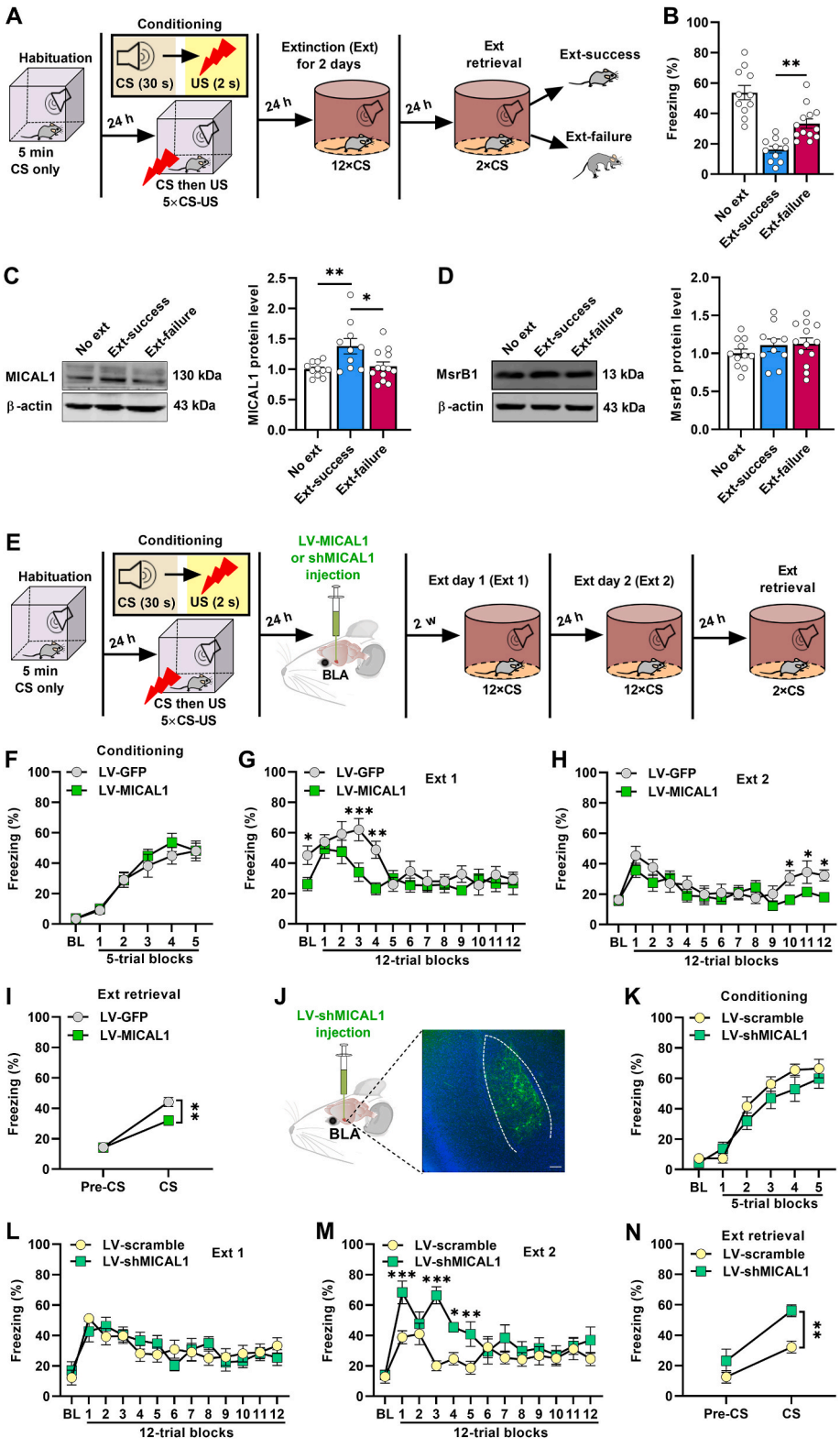

(caption on next page)

Fig. 4. Overexpression of MICAL1 in BLA facilitates the extinction of cued fear memory. (A) Behavioral scheme for extinction. (B) Extinction success mice displayed a better performance on extinction retrieval compared to those that experienced extinction failure mice (n = 11–13 mice per group). (C) The expression of MICAL1 in the BLA was found to be upregulated in extinction success mice, (D) whereas MsrB1 did not show similar changes (n = 10–13 mice per group). (E) Schematic of the experimental design. (F) The LV-GFP and LV-MICAL1 groups exhibited an equivalent fear acquisition during conditioning (n = 10–11 mice per group). (G, H) The LV-MICAL1 group showed a better extinction learning on both day 1 and day 2 (n = 10–11 mice per group). (I) The LV-MICAL1 group displayed a significant reduction in freezing behavior on extinction retrieval (n = 10–11 mice per group). (J) Representative fluorescence image for LV-shMICAL1 expression in the BLA. (K) Both of the LV-scramble and LV-shMICAL1 groups showed an equivalent fear acquisition during conditioning (n = 8–9 mice per group). (L, M) The LV-shMICAL1 group showed an increased freezing level during extinction learning on day 2, but not on day 1 (n = 8–9 mice per group). (N) The LV-shMICAL1 group displayed an increased freezing level on extinction retrieval (n = 8–9 mice per group). Ext: Extinction; Ext-success: Extinction success; Ext-failure: Extinction failure; No ext: no extinction. One-way ANOVA with Tukey's multiple comparisons tests (B-D); two-way ANOVA with Bonferroni's multiple comparisons post hoc tests (F, I, K, N); two-way ANOVA with Fisher's LSD tests (G, H, L, M). $^{*}p < 0.05$, $^{**}p < 0.01$ and $^{***}p < 0.001$. Data are presented as the mean ± SEM.

3.7. MICAL1 reactivation in a short window rapidly disrupts cued fear memory

Physically, the enzymatic activity of MICALs is auto-inhibited by their C-terminal domain [39,40]. Previous studies have reported that the autoinhibition of MICAL1 are released by SEMAs, which are classified into eight classes (classes 1-7 and class V) based on their structural domain features [41-43]. Consequently, recombinant mouse SEMA3A was utilized as an activator of MICAL1 to examine whether reactivation of MICAL1 within a specific time window could rapidly suppress fear memory. Mice were bilaterally implanted with cannulas positioned above the BLA. After one week recovery, the mice that underwent cued fear conditioning were subsequently injected with either vehicle or recombinant mouse SEMA3A into BLA at different time points (Fig. 7A). Notably, SEMA3A administered 0.5 h after cued fear conditioning significantly disrupted fear memory, as indicated by a reduced freezing response during cued fear memory retrieval (Fig. 7B), whereas minimal differences were observed at other time points (Fig. 7C-E). Taken together, our data indicate that acquired traumatic memory may be rapidly disrupted by the reactivation of MICAL1 within a short time window.

4. Discussion

In recent decades, extensive efforts have been made to erase negative emotion memories as a treatment for memory-based disorders. Altered dendritic spine plasticity and cytoskeleton dynamics in the BLA have been implicated in the fear memory retention, however, the underlying mechanisms have not been fully clarified. Herein, we discovered a causal role of redox-dependent cytoskeleton dynamics underlying fear memory retention and extinction (Fig. 8). Our findings indicated that deficits in the oxidation dynamics of F-actin in the BLA contributed to the persistence of fear-associated morphological changes in dendritic spines. Moreover, targeting cytoskeleton reorganization by promoting F-actin methionine oxidation disrupted fear memory retention and facilitated extinction.

It has long been recognized that fear conditioning increases the numbers of dendritic spine and dendritic intersections in the BLA, a critical site of plasticity for extinction [4,44]. A reversal of fear conditioning-induced alterations in the BLA dendritic plasticity has been considered to mimic the behavioral consequences of extinction learning [45]. Mushroom-shaped dendritic spines are characterized by a high enrichment of F-actin, and recognized as mature and stable structures, which often referred to as 'memory spines' [46,47]. A recent study has reported that decreasing F/G-actin ratio by knockdown of an RNA-binding protein, fragile X messenger ribonucleoprotein 1, reduced the ratio of mature spines versus immature spines [48]. In our current study, we also observed a decreased F/G-actin ratio in Ext mice (Fig. 1M), which were accompanied by a reduction in mushroom-like dendritic spines. Collectively, it can be speculated that F/G-actin conversion may preferentially affect mushroom-like dendritic spines, although the precise mechanisms require further investigation.

Using phalloidin staining, we observed an increase in actin filaments and spine numbers in the BLA following fear conditioning, while subsequent extinction training reversed these effects, supporting the view that synaptic plasticity events in the BLA may drive fear memory retention. However, the molecular mechanisms underlying fear conditioning-induced alterations in dendritic plasticity remain poorly understood. We identified that MICAL1, an emerging factor involved in F-actin disassembly, works as a central player underlying fear memory-related actin dynamics. Actin's ability to polymerize into dynamic filaments is critical for the plasticity of dendritic spines.

Interestingly, the polymerization of F-actin is susceptible to the redox modifications of their methionine residues. MICAL1, a cytoplasmic protein characterized by a highly conserved flavoprotein monooxygenase enzymatic domain, directly destabilizes F-actin via stereospecific oxidation. Over the past decade, numerous work has highlighted the importance of MICAL1 in many cellular events such as cell division, vesicle cargo, cell migration, and cell growth [10,11,49]. Until now, to our knowledge, little is known about the role of MICAL1 in behavioral regulation. Herein, we observed that the expression of MICAL1 in the BLA was down-regulated rapidly after fear conditioning, accompanied by a reduction of oxidized F-actin and an increase in MsrB1, a key enzyme responsible for recovering oxidized F-actin monomer. It should be noted that stress was discovered to decrease the level of MICAL1, which may be involved in the process of stress-enhanced fear learning. Following fear conditioning, overexpression of MICAL1 in the BLA re-activated cytoskeleton remodeling and refreshed the spine morphology, indicating that deficits in the oxidation dynamics of F-actin may confer to the sustained morphological changes in the BLA induced by fear conditioning. Overexpression of MICAL1 did not affect the spine density and dendritic retraction in the BLA of control mice, but it reduced the spine density in the conditioned mice. One possible explanation is that, the monooxygenase activity of MICAL1 is controlled by F-actin content. The increased actin filaments after fear conditioning may amplify the effect of MICAL1 overexpression.

Some anti-cancer drugs, such as vincristine and paclitaxel, achieve therapeutic effects in clinical practice via affecting cytoskeleton, and the actin cytoskeleton has been considered as a potential therapeutic target for cancer [50-52]. Actin provides the structural underpinnings for the morphological plasticity of dendritic spines. Given a key role of actin cytoskeleton dynamics in spine plasticity, the actin cytoskeleton has also been raised as a potential target for addressing methamphetamine relapse and morphine withdrawal symptoms. In recent years, much attention has been paid on the role of major regulatory factors influencing actin dynamics, such as myosin II, cofilin 1 and LIM kinase, in the fear memory process. Both pharmacological depolymerization of actin filaments and optical erasure of cofilactin, the main stabilizing factor of actin filaments, have been found to disrupt memory consolidation, raising the possibility that the arrest of actin filaments may lead to fear memory retention [53-55]. Our findings indicate that, similar to the effects of pharmacological depolymerization, overexpression of MICAL1 in the BLA after fear conditioning not only facilitated the extinction learning, as evidenced by a decreased freezing behavior in the early trial blocks on day 1 of extinction learning (Fig. 4G), but also helped stabilize the newly formed extinction memory, as indicated by a reduced freezing behavior in the later trial blocks on day 2 of extinction learning

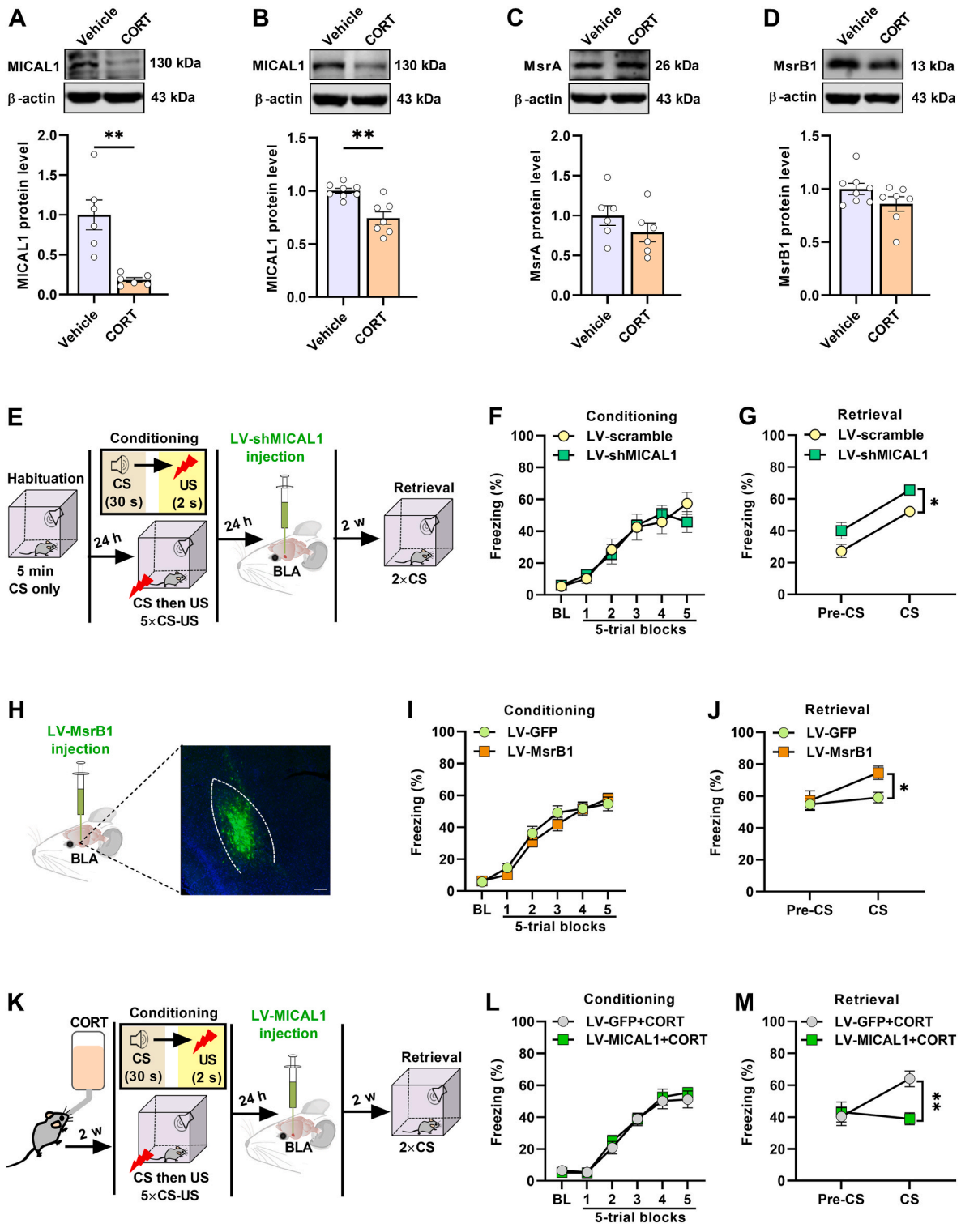

Fig. 5. Corticosterone-altered MICAL1 expression is involved in the PTSD-like memories. (A) Incubation of HT22 cells with CORT (1 μM) for 24 h resulted in a decreased expression of MICAL1 (n = 6 cells per group). (B) Exposure of CORT (5 mg/kg) over two weeks resulted in a decreased expression of MICAL1 in the BLA of mice (n = 7–8 mice per group). (C, D) No significant differences were observed in the expression levels of (C) MsrA and (D) MsrB1 between vehicle and CORT-exposed mice in the BLA (n = 6–8 mice per group). (E) Schematic of the experimental design. (F) The LV-scramble and LV-shMICAL1 groups showed a similar fear response during conditioning (n = 8 mice per group). (G) Knockdown of MICAL1 in the BLA resulted in an increased freezing behavior on retrieval (n = 16–17 mice per group). (H) Representative fluorescence image from the BLA of the LV-MsrB1 group. (I) The LV-GFP and LV-MsrB1 groups exhibited similar levels of accumulated freezing during conditioning (n = 16 mice per group). (J) Overexpression of MsrB1 in the BLA resulted in an increased freezing behavior on retrieval (n = 14–16 mice per group). (K) Schematic of the experimental design. (L) CORT-exposed mice exhibited an equivalent fear response during conditioning. (M) Overexpression of MICAL1 in the BLA reversed the increased fear response on retrieval in CORT-exposed mice (n = 10 mice per group). CORT: corticosterone. Two-tailed, unpaired *t*-test with Welch's correction (A, B); two-tailed, unpaired *t* tests (C, D); two-way ANOVA with Bonferroni's multiple comparisons post hoc tests (F, G, I, J, L, M). $*p < 0.05$, $**p < 0.01$. Data are presented as the mean ± SEM.

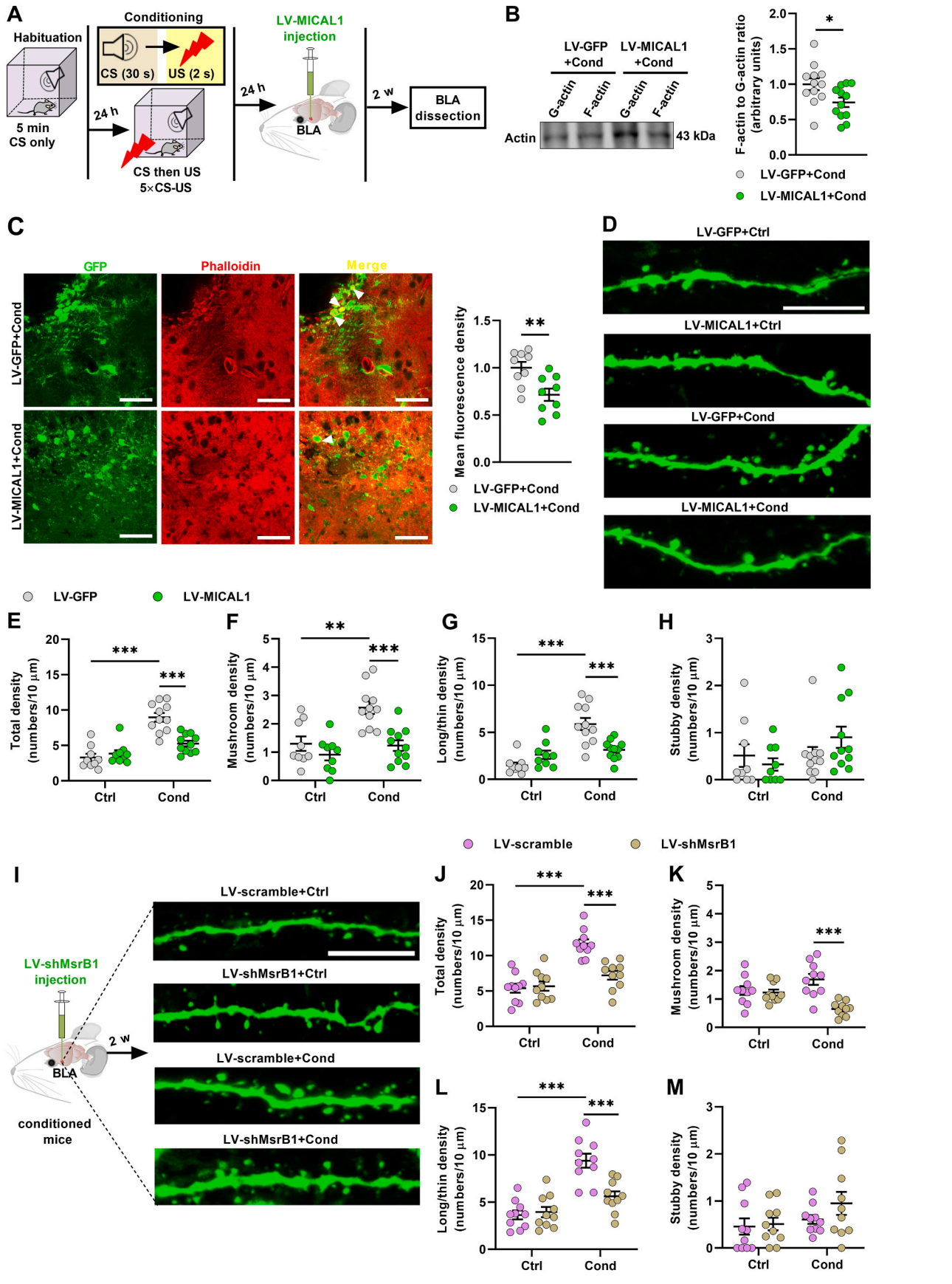

(caption on next page)

Fig. 6. MICAL1-mediated methionine oxidation of actin cytoskeleton reverses fear conditioning-induced increase in dendritic spines in BLA. (A) Schematic of the experimental design. (B) Overexpression of MICAL1 in the BLA decreased the ratio of F-actin to G-actin in conditioned mice (n = 12 mice per group). (C) Overexpression of MICAL1 in the BLA reduced the fluorescence density of F-actin in conditioned mice (n = 9 slices from 3 mice per group). Scale bars: 50 μm. (D) Representative images of dendritic spines from BLA neurons were displayed for the LV-GFP and LV-MICAL1 groups in control and conditioned mice. Scale bars: 10 μm. (E-H) Overexpression of MICAL1 in the BLA reversed the increases in (E) total, (F) mushroom-, and (G) long/thin-shaped spines density in conditioned mice, while having no effect on (H) stubby-shaped spines (n = 9–11 neurons from 3 mice per group). (I) Representative images of dendritic spines in the BLA neurons were obtained from the LV-scramble and LV-shMsrB1 groups of control and conditioned mice. Scale bars: 10 μm. (J-M) Knockdown of MsrB1 in the BLA reversed the increases in (J) total, (K) mushroom-, and (L) long/thin-shaped spines density in conditioned mice, without affecting (M) stubby-shaped spines (n = 10 neurons from 3 mice per group). Ctrl: control; Cond: conditioned. Two-tailed, unpaired *t* tests (B, C); two-way ANOVA with Bonferroni's multiple comparisons post hoc tests (E-H and J-M). $*p < 0.05$, $**p < 0.01$ and $***p < 0.001$. Data are presented as the mean ± SEM.

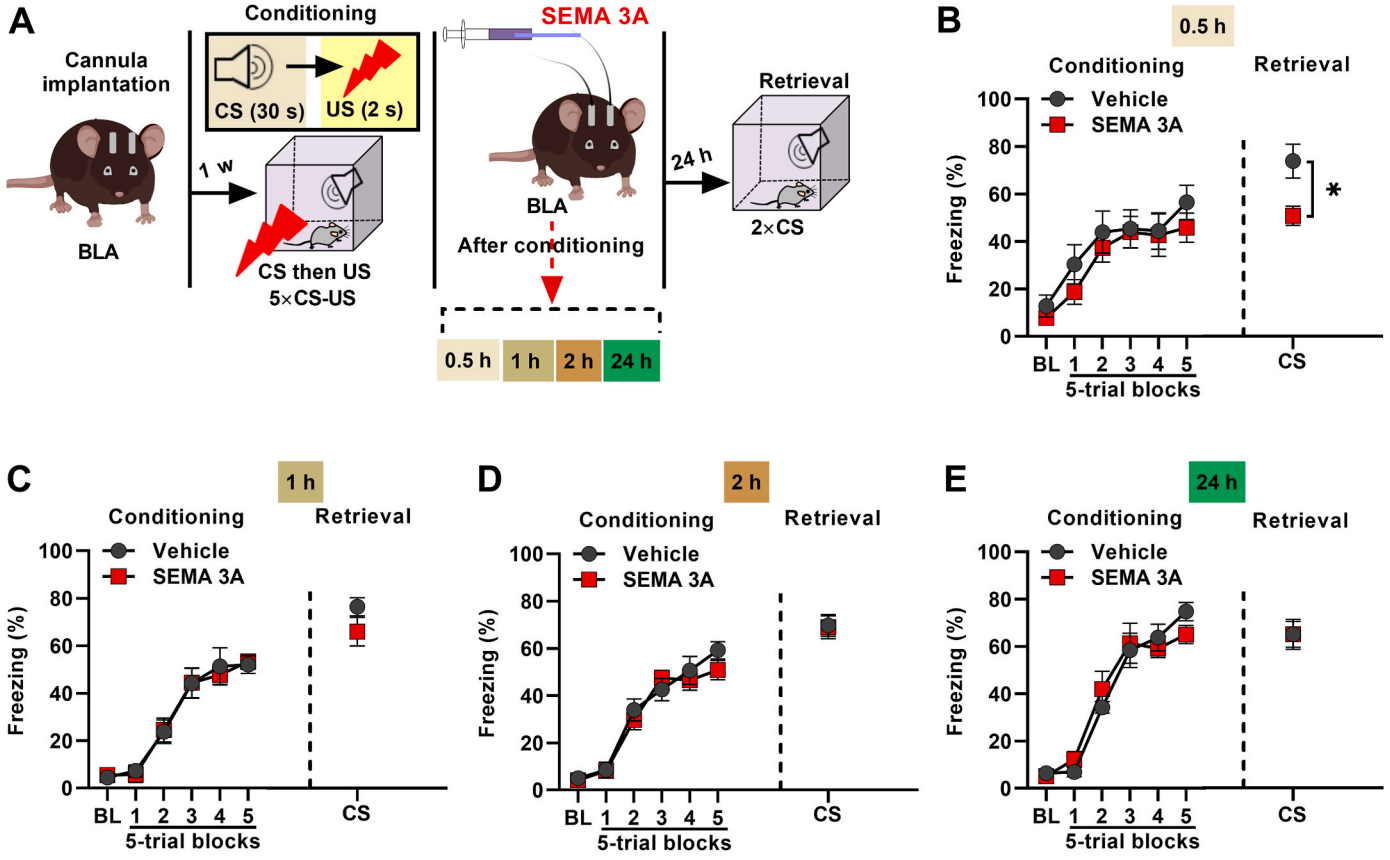

Fig. 7. MICAL1 reactivation in a short window rapidly disrupts cued fear memory. (A) Schematic of the experimental design. (B-E) The effect of MICAL1 reactivation by recombinant mouse SEMA3A on fear memory retrieval was examined. Injection of recombinant mouse SEMA3A into the BLA at (B) 0.5 h, but not at (C) 1 h, (D) 2 h and (E) 24 h post-conditioning, significantly attenuated freezing behavior on retrieval (n = 8 mice per group). Two-way ANOVA with Bonferroni's multiple comparisons post hoc tests (left) or two-tailed, unpaired *t* tests (right) (B-E). $*p < 0.05$. Data are presented as the mean ± SEM.

(Fig. 4H). Furthermore, intra-BLA injection of recombinant SEMA3A, an activator that releases MICAL1 from autoinhibition through transmembrane plexin receptor, rapidly disrupted fear memory consolidation in a short time window after traumatic stress. These data strongly support the hypothesis that modification to actin filaments may in favor of the erasure of negative memories.

Our data reveals an unexpected role for oxidoreduction in triggering actin depolymerization to control fear memory process. Although reactive oxygen species at non-physiological levels are well known to impair memory and synaptic plasticity, it has been recognized for long that the reversible oxidation/reduction of specific amino acid mediates signaling transduction and plays a physiological role in regulating synaptic plasticity [56-59]. A lot of evidence supports that MICALs-mediated oxidation is crucial for their actin-regulatory function [6,60,61]. Remarkably, MICAL1 oxidize two specific actin methionine, Met 44 and Met 47, which are located in an important region involved in actin subunit interactions [62]. It should be noted that MICALs have also been found to release the diffusible oxidant H_2O_2, and despite the MICALs, ROS is also shown to depolymerize the actin cytoskeleton via modification of various amino acid residues [14,63], including methionine residues. Our previous study reported that excess oxidative stress in the BLA impairs fear extinction via oxidizing N-methyl-D-aspartic acid receptors [64]. Current data leaves a broader opening for investigating the relationship between non-enzymatic oxidation of F-actin by means of ROS and specific enzymatic oxidation by MICAL1 in the process of fear memory.

The present study has certain limitations. First, our findings indicate that, compared to the no extinction group, the Ext-success mice displayed a reduced dendritic spines density (Fig. 1I). However, the dendritic spines density of the Ext-failure mice has not been undetermined in the current study. Additionally, we utilized a lentiviral vector harboring the shRNA sequence specifically targeting the MsrB1 gene. Nevertheless, the consequential impact of this gene knockdown on other redox enzymes, such as MICAL1, are not addressed in the study and warrant further investigation. Although MICAL1 is widely thought to selectively target actin, a recent study has demonstrated that MICAL1

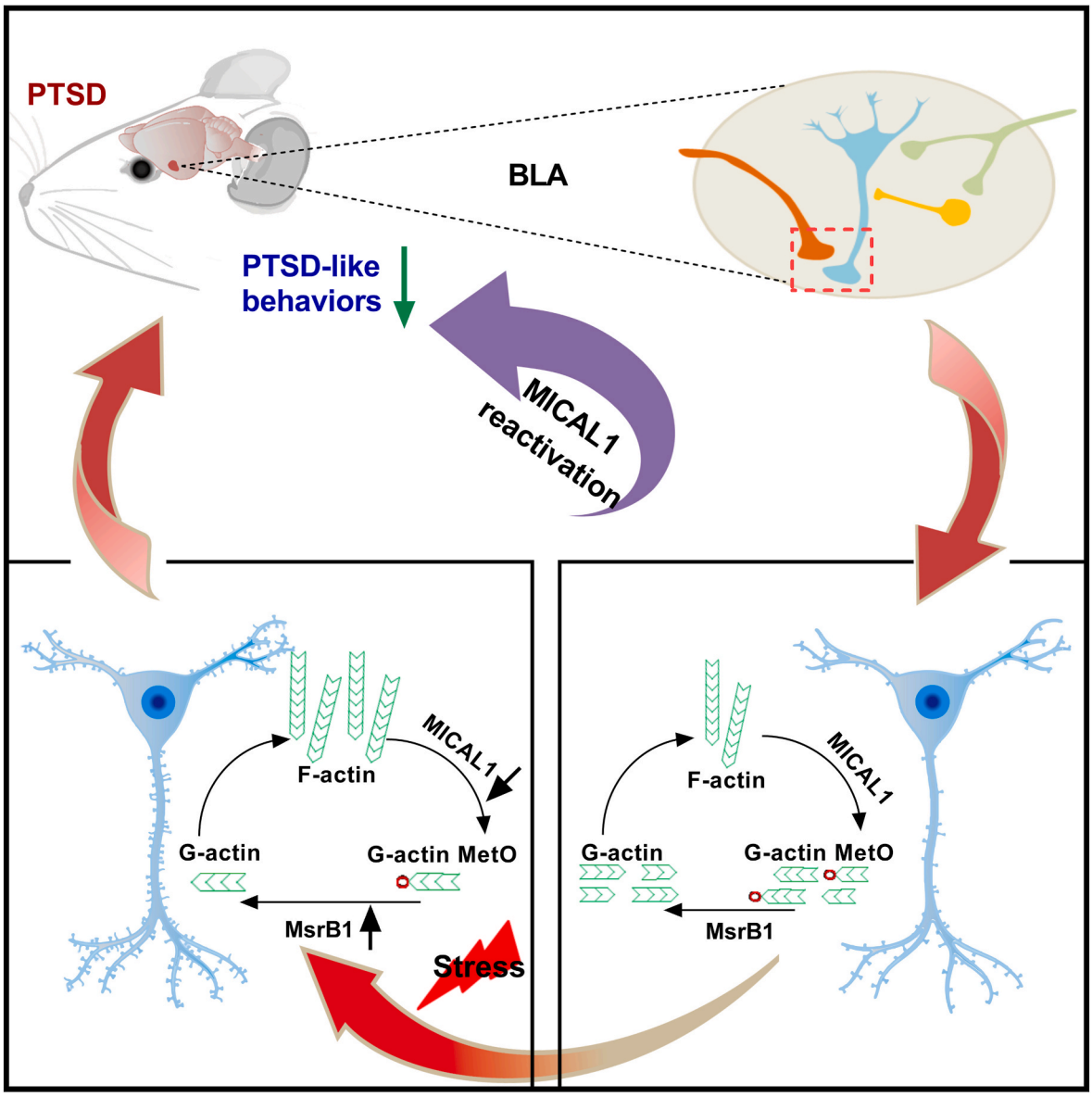

Fig. 8. A working model illustrating how F-actin methionine oxidation dynamics regulates traumatic memories. Traumatic events lead to a down-regulation of MICAL1 expression and an up-regulation of MsrB1 expression in the BLA, resulting in a decrease in F-actin methionine oxidation and an increase in dendritic spine density, which confers long-lasting retention of traumatic memories. Re-activation of MICAL1 counteracts the increase in the actin assembly and dendritic spine complexity in the BLA, thereby inhibiting the retention of traumatic memories.

oxidizes methionine at site 308 in Ca^{2+}/calmodulin-dependent protein kinase II (CaMKII), thereby reducing its activity, while MsrB1 serves to reduce this oxidation [65]. CaMKII activity is essential for the regulation of dendritic spines plasticity and actin polymerization [66-68]. Decreased CaMKII activity subsequently inhibits LIM kinases-mediated phosphorylation of serine 3 on cofilin, a critical F-actin side-binding protein that accumulates at the base of spine head, which may promote the turnover of F/G-actin [69,70]. Therefore, the role of MICAL1-catalyzed oxidation of CaMKII in the traumatic memory retention remains to be assessed.

5. Conclusion

Our results identified an important redox-dependent mechanism that regulates fear memory retention and provided further evidence for the importance of actin cytoskeleton-dependent synaptic plasticity events in memory-based disorders. Future studies should reveal the functional relationship between the MICAL1 and ROS-mediated protein translational modifications in the control of memory, which may provide a redox perspective for understanding how the traumatic experience shape aversive memories, and identify new potential therapeutic interventions against emotion disorders by targeting cytoskeleton.

Funding

This work was supported by the following grants: National Science and Technology Major Project of China (2021ZD0202900); National Natural Science Foundation of China (82373858, 82130110, U21A20363); Innovative Research Groups of National Natural Science Foundation of China (81721005).

CRediT authorship contribution statement

Cun-Dong Huang: Writing – original draft, Methodology, Investigation, Formal analysis, Data curation. **Yu Shi:** Investigation, Formal analysis. **Fang Wang:** Writing – review & editing, Supervision, Project

administration, Funding acquisition, Conceptualization. **Peng-Fei Wu:** Writing – review & editing, Writing – original draft, Supervision, Resources, Conceptualization. **Jian-Guo Chen:** Writing – review & editing, Supervision, Funding acquisition, Conceptualization.

Declaration of competing interest

The authors declare that they have no known competing financial interests or personal relationships that could have appeared to influence the work reported in this paper.

Appendix A. Supplementary data

Supplementary data to this article can be found online at https://doi.org/10.1016/j.redox.2024.103391.

Data availability

Data will be made available on request.

References

[1] G.J. Quirk, D. Mueller, Neural mechanisms of extinction learning and retrieval, Neuropsychopharmacology 33 (1) (2008) 56–72, https://doi.org/10.1038/sj.npp.1301555.

[2] C. Furini, J. Myskiw, I. Izquierdo, The learning of fear extinction, Neurosci. Biobehav. Rev. 47 (2014) 670–683, https://doi.org/10.1016/j.neubiorev.2014.10.016.

[3] M. Maroun, P.J. Ioannides, K.L. Bergman, et al., Fear extinction deficits following acute stress associate with increased spine density and dendritic retraction in basolateral amygdala neurons, Eur. J. Neurosci. 38 (4) (2013) 2611–2620, https://doi.org/10.1111/ejn.12259.

[4] S.C. Heinrichs, K.A. Leite-Morris, M.D. Guy, et al., Dendritic structural plasticity in the basolateral amygdala after fear conditioning and its extinction in mice, Behav. Brain Res. 248 (2013) 80–84, https://doi.org/10.1016/j.bbr.2013.03.048.

[5] E. Tsvetkov, W.A. Carlezon, F.M. Benes, et al., Fear conditioning occludes LTP-induced presynaptic enhancement of synaptic transmission in the cortical pathway to the lateral amygdala, Neuron 34 (2) (2002) 289–300, https://doi.org/10.1016/s0896-6273(02)00645-1.

[6] R.-J. Hung, C.W. Pak, J.R. Terman, Direct redox regulation of F-actin assembly and disassembly by Mical, Science 334 (6063) (2011) 1710–1713, https://doi.org/10.1126/science.1211956.

[7] R.-J. Hung, C.S. Spaeth, H.G. Yesilyurt, et al., SelR reverses Mical-mediated oxidation of actin to regulate F-actin dynamics, Nat. Cell Biol. 15 (12) (2013) 1445–1454, https://doi.org/10.1038/ncb2871.

[8] S. Rajan, J.R. Terman, E. Reisler, MICAL-mediated oxidation of actin and its effects on cytoskeletal and cellular dynamics, Front. Cell Dev. Biol. 11 (2023) 1124202, https://doi.org/10.3389/fcell.2023.1124202.

[9] E.Y. Van Battum, R.-A.F. Gunput, S. Lemstra, et al., The intracellular redox protein MICAL-1 regulates the development of hippocampal mossy fibre connections, Nat. Commun. 5 (2014) 4317, https://doi.org/10.1038/ncomms5317.

[10] D.J. McGarry, G. Armstrong, G. Castino, et al., MICAL1 regulates actin cytoskeleton organization, directional cell migration and the growth of human breast cancer cells as orthotopic xenograft tumours, Cancer Lett. 519 (2021) 226–236, https://doi.org/10.1016/j.canlet.2021.07.039.

[11] F. Niu, K. Sun, W. Wei, et al., F-actin disassembly factor MICAL1 binding to Myosin Va mediates cargo unloading during cytokinesis, Sci. Adv. 6 (45) (2020), https://doi.org/10.1126/sciadv.abb1307.

[12] M.R. Lundquist, A.J. Storaska, T.-C. Liu, et al., Redox modification of nuclear actin by MICAL-2 regulates SRF signaling, Cell 156 (3) (2014) 563–576, https://doi.org/10.1016/j.cell.2013.12.035.

[13] K. Tominaga, H. Minato, T. Murayama, et al., Semaphorin signaling via MICAL3 induces symmetric cell division to expand breast cancer stem-like cells, Proc. Natl. Acad. Sci. U.S.A. 116 (2) (2019) 625–630, https://doi.org/10.1073/pnas.1806851116.

[14] E.E. Grintsevich, P. Ge, M.R. Sawaya, et al., Catastrophic disassembly of actin filaments via Mical-mediated oxidation, Nat. Commun. 8 (1) (2017) 2183, https://doi.org/10.1038/s41467-017-02357-8.

[15] E.E. Grintsevich, H.G. Yesilyurt, S.K. Rich, et al., F-actin dismantling through a redox-driven synergy between Mical and cofilin, Nat. Cell Biol. 18 (8) (2016) 876–885, https://doi.org/10.1038/ncb3390.

[16] S. Rajan, J. Yoon, H. Wu, et al., Disassembly of bundled F-actin and cellular remodeling via an interplay of Mical, cofilin, and F-actin crosslinkers, Proc. Natl. Acad. Sci. U.S.A. 120 (39) (2023) e2309955120, https://doi.org/10.1073/pnas.2309955120.

[17] B.C. Lee, Z. Péterfi, F.W. Hoffmann, et al., MsrB1 and MICALs regulate actin assembly and macrophage function via reversible stereoselective methionine oxidation, Mol. Cell. 51 (3) (2013) 397–404, https://doi.org/10.1016/j.molcel.2013.06.019.

[18] E.J. Young, H. Lin, T.M. Kamenecka, et al., Methamphetamine learning induces persistent and selective nonmuscle myosin II-dependent spine motility in the basolateral amygdala, J. Neurosci. 40 (13) (2020) 2695–2707, https://doi.org/10.1523/JNEUROSCI.2182-19.2020.

[19] M. Hafenbreidel, S. Pandey, S.B. Briggs, et al., Basolateral amygdala corticotropin releasing factor receptor 2 interacts with nonmuscle myosin II to destabilize memory in males, Neurobiol. Learn. Mem. 206 (2023) 107865, https://doi.org/10.1016/j.nlm.2023.107865.

[20] R. Lamprecht, The role of actin cytoskeleton in memory formation in amygdala, Front. Mol. Neurosci. 9 (2016) 23, https://doi.org/10.3389/fnmol.2016.00023.

[21] H.-Y. Zhou, J.-G. He, Z.-L. Hu, et al., A-kinase anchoring protein 150 and protein kinase a complex in the basolateral amygdala contributes to depressive-like behaviors induced by chronic restraint stress, Biol. Psychiatr. 86 (2) (2019) 131–142, https://doi.org/10.1016/j.biopsych.2019.03.967.

[22] F.-F. Chen, C.-M. Wang, H.-S. Chen, et al., SKF83959, an agonist of phosphatidylinositol-linked dopamine receptors, prevents renewal of extinguished conditioned fear and facilitates extinction, Brain Res. 1749 (2020) 147136, https://doi.org/10.1016/j.brainres.2020.147136.

[23] K. Li, H.-S. Chen, D. Li, et al., SAR405, a highly specific VPS34 inhibitor, disrupts auditory fear memory consolidation of mice via facilitation of inhibitory neurotransmission in basolateral amygdala, Biol. Psychiatr. 85 (3) (2019) 214–225, https://doi.org/10.1016/j.biopsych.2018.07.026.

[24] X.-P. Yao, J. Ye, T. Feng, et al., Adaptor protein MyD88 confers the susceptibility to stress via amplifying immune danger signals, Brain Behav. Immun. 108 (2023) 204–220, https://doi.org/10.1016/j.bbi.2022.12.007.

[25] J. Morandell, L.A. Schwarz, B. Basilico, et al., Cul 3 regulates cytoskeleton protein homeostasis and cell migration during a critical window of brain development, Nat. Commun. 12 (1) (2021) 3058, https://doi.org/10.1038/s41467-021-23123-x.

[26] R. Rosas-Hernández, Y. Bastián, A. Juárez Tello, et al., AMPA receptors modulate the reorganization of F-actin in Bergmann glia cells through the activation of RhoA, J. Neurochem. 149 (2) (2019) 242–254, https://doi.org/10.1111/jnc.14658.

[27] Q.-Q. Han, P.-F. Wu, Y.-H. Li, et al., SVCT2-mediated ascorbic acid uptake buffers stress responses via DNA hydroxymethylation reprogramming of S100 calcium-binding protein A4 gene, Redox Biol. 58 (2022) 102543, https://doi.org/10.1016/j.redox.2022.102543.

[28] W. Sun, Z. Liu, X. Jiang, et al., Spatial transcriptomics reveal neuron-astrocyte synergy in long-term memory, Nature 627 (8003) (2024) 374–381, https://doi.org/10.1038/s41586-023-07011-6.

[29] O. Gunduz-Cinar, L.I. Castillo, M. Xia, et al., A cortico-amygdala neural substrate for endocannabinoid modulation of fear extinction, Neuron 111 (19) (2023), https://doi.org/10.1016/j.neuron.2023.06.023.

[30] L.T. Neves, P.F.R. Neves, L.V. Paz, et al., Increases in dendritic spine density in BLA without metabolic changes in a rodent model of PTSD, Brain Struct. Funct. 224 (8) (2019) 2857–2870, https://doi.org/10.1007/s00429-019-01943-4.

[31] L.A. Cingolani, Y. Goda, Actin in action: the interplay between the actin cytoskeleton and synaptic efficacy, Nat. Rev. Neurosci. 9 (5) (2008) 344–356, https://doi.org/10.1038/nrn2373.

[32] P. Hotulainen, C.C. Hoogenraad, Actin in dendritic spines: connecting dynamics to function, J. Cell Biol. 189 (4) (2010) 619–629, https://doi.org/10.1083/jcb.201003008.

[33] C. Herry, F. Ferraguti, N. Singewald, et al., Neuronal circuits of fear extinction, Eur. J. Neurosci. 31 (4) (2010) 599–612, https://doi.org/10.1111/j.1460-9568.2010.07101.x.

[34] E. Knapska, M. Macias, M. Mikosz, et al., Functional anatomy of neural circuits regulating fear and extinction, Proc. Natl. Acad. Sci. U.S.A. 109 (42) (2012) 17093–17098, https://doi.org/10.1073/pnas.1202087109.

[35] J.-M. Revest, F. Di Blasi, P. Kitchener, et al., The MAPK pathway and Egr-1 mediate stress-related behavioral effects of glucocorticoids, Nat. Neurosci. 8 (5) (2005) 664–672, https://doi.org/10.1038/nn1441.

[36] R. Inagaki, S. Moriguchi, K. Fukunaga, Aberrant amygdala-dependent fear memory in corticosterone-treated mice, Neuroscience 388 (2018) 448–459, https://doi.org/10.1016/j.neuroscience.2018.08.004.

[37] M.A. Lynch, Long-term potentiation and memory, Physiol. Rev. 84 (1) (2004), https://doi.org/10.1152/physrev.00014.2003.

[38] J. Noguchi, T. Hayama, S. Watanabe, et al., State-dependent diffusion of actin-depolymerizing factor/cofilin underlies the enlargement and shrinkage of dendritic spines, Sci. Rep. 6 (2016) 32897, https://doi.org/10.1038/srep32897.

[39] S. Frémont, H. Hammich, J. Bai, et al., Oxidation of F-actin controls the terminal steps of cytokinesis, Nat. Commun. 8 (2017) 14528, https://doi.org/10.1038/ncomms14528.

[40] T. Vitali, E. Maffioli, G. Tedeschi, et al., Properties and catalytic activities of MICAL1, the flavoenzyme involved in cytoskeleton dynamics, and modulation by its CH, LIM and C-terminal domains, Arch. Biochem. Biophys. 593 (2016) 24–37, https://doi.org/10.1016/j.abb.2016.01.016.

[41] R.-J. Hung, U. Yazdani, J. Yoon, et al., Mical links semaphorins to F-actin disassembly, Nature 463 (7282) (2010) 823–827, https://doi.org/10.1038/nature08724.

[42] R.-J. Hung, J.R. Terman, Extracellular inhibitors, repellents, and semaphorin/plexin/MICAL-mediated actin filament disassembly, Cytoskeleton (Hoboken) 68 (8) (2011) 415–433, https://doi.org/10.1002/cm.20527.

[43] E.F. Schmidt, S.-O. Shim, S.M. Strittmatter, Release of MICAL autoinhibition by semaphorin-plexin signaling promotes interaction with collapsin response mediator protein, J. Neurosci. 28 (9) (2008) 2287–2297, https://doi.org/10.1523/JNEUROSCI.5646-07.2008.

[44] K.M. Hagihara, O. Bukalo, M. Zeller, et al., Intercalated amygdala clusters orchestrate a switch in fear state, Nature 594 (7863) (2021) 403–407, https://doi.org/10.1038/s41586-021-03593-1.
[45] D. Laricchiuta, J. Gimenez, G. Sciamanna, et al., Synaptic and transcriptomic features of cortical and amygdala pyramidal neurons predict inefficient fear extinction, Cell Rep. 42 (9) (2023) 113066, https://doi.org/10.1016/j.celrep.2023.113066.
[46] H. Kasai, M. Matsuzaki, J. Noguchi, et al., Structure-stability-function relationships of dendritic spines, Trends Neurosci. 26 (7) (2003) 360–368, https://doi.org/10.1016/S0166-2236(03)00162-0.
[47] S. Miyata, M. Tsuda, S. Mitsui, Overexpression of motopsin, an extracellular serine protease related to intellectual disability, promotes adult neurogenesis and neuronal responsiveness in the dentate gyrus, Mol. Neurobiol. 61 (8) (2024) 4929–4948, https://doi.org/10.1007/s12035-023-03890-y.
[48] V. Mercaldo, B. Vidimova, D. Gastaldo, et al., Altered striatal actin dynamics drives behavioral inflexibility in a mouse model of fragile X syndrome, Neuron 111 (11) (2023), https://doi.org/10.1016/j.neuron.2023.03.008.
[49] L.T. Alto, J.R. Terman, MICALs, Curr. Biol. 28 (9) (2018) R538–R541, https://doi.org/10.1016/j.cub.2018.01.025.
[50] Q. Wang, H. Wu, J. Hu, et al., Nestin is required for spindle assembly and cell-cycle progression in glioblastoma cells, Mol. Cancer Res. 19 (10) (2021) 1651–1665, https://doi.org/10.1158/1541-7786.MCR-20-0994.
[51] M. Lončarić, N. Stojanović, A. Rac-Justament, et al., Talin 2 and KANK2 functionally interact to regulate microtubule dynamics, paclitaxel sensitivity and cell migration in the MDA-MB-435S melanoma cell line, Cell. Mol. Biol. Lett. 28 (1) (2023) 56, https://doi.org/10.1186/s11658-023-00473-6.
[52] X. Xu, S. Xu, J. Wan, et al., Disturbing cytoskeleton by engineered nanomaterials for enhanced cancer therapeutics, Bioact. Mater. 29 (2023) 50–71, https://doi.org/10.1016/j.bioactmat.2023.06.016.
[53] C. Medina, V. de la Fuente, S. Tom Dieck, et al., LIMK, Cofilin 1 and actin dynamics involvement in fear memory processing, Neurobiol. Learn. Mem. 173 (2020) 107275, https://doi.org/10.1016/j.nlm.2020.107275.
[54] A. Goto, A. Bota, K. Miya, et al., Stepwise synaptic plasticity events drive the early phase of memory consolidation, Science 374 (6569) (2021) 857–863, https://doi.org/10.1126/science.abj9195.
[55] K. Rehberg, J.R. Bergado-Acosta, J.C. Koch, et al., Disruption of fear memory consolidation and reconsolidation by actin filament arrest in the basolateral amygdala, Neurobiol. Learn. Mem. 94 (2) (2010) 117–126, https://doi.org/10.1016/j.nlm.2010.04.007.
[56] P. Wang, F. Wang, L. Ni, et al., Targeting redox-altered plasticity to reactivate synaptic function: a novel therapeutic strategy for cognitive disorder, Acta Pharm. Sin. B 11 (3) (2021) 599–608, https://doi.org/10.1016/j.apsb.2020.11.012.
[57] A. Kamsler, M. Segal, Hydrogen peroxide modulation of synaptic plasticity, J. Neurosci. 23 (1) (2003) 269–276, https://doi.org/10.1523/JNEUROSCI.23-01-00269.2003.
[58] L.T. Knapp, E. Klann, Potentiation of hippocampal synaptic transmission by superoxide requires the oxidative activation of protein kinase C, J. Neurosci. 22 (3) (2002) 674–683, https://doi.org/10.1523/JNEUROSCI.22-03-00674.2002.
[59] A.T. Huddleston, W. Tang, H. Takeshima, et al., Superoxide-induced potentiation in the hippocampus requires activation of ryanodine receptor type 3 and ERK, J. Neurophysiol. 99 (3) (2008) 1565–1571, https://doi.org/10.1152/jn.00659.2007.
[60] S.S.P. Giridharan, J.L. Rohn, N. Naslavsky, et al., Differential regulation of actin microfilaments by human MICAL proteins, J. Cell Sci. 125 (Pt 3) (2012) 614–624, https://doi.org/10.1242/jcs.089367.
[61] J. Yoon, R.-J. Hung, J.R. Terman, Characterizing F-actin disassembly induced by the semaphorin-signaling component MICAL, Methods Mol. Biol. 1493 (2017) 119–128, https://doi.org/10.1007/978-1-4939-6448-2_8.
[62] R. Dominguez, K.C. Holmes, Actin structure and function, Annu. Rev. Biophys. 40 (2011) 169–186, https://doi.org/10.1146/annurev-biophys-042910-155359.
[63] Y. Zhang, R. Xu, J. Wu, et al., Nanopore-related cellular death through cytoskeleton depolymerization by drug-induced ROS, Talanta 268 (Pt 2) (2024) 125355, https://doi.org/10.1016/j.talanta.2023.125355.
[64] P.-F. Wu, X.-L. Guan, F. Wang, et al., N-acetylcysteine facilitates extinction of cued fear memory in rats via reestablishing basolateral amygdala glutathione homeostasis, Acta Pharmacol. Sin. 43 (2) (2022) 260–272, https://doi.org/10.1038/s41401-021-00661-0.
[65] K. Konstantinidis, V.J. Bezzerides, L. Lai, et al., MICAL1 constrains cardiac stress responses and protects against disease by oxidizing CaMKII, J. Clin. Invest. 130 (9) (2020) 4663–4678, https://doi.org/10.1172/JCI133181.
[66] R. Yasuda, Y. Hayashi, J.W. Hell, CaMKII: a central molecular organizer of synaptic plasticity, learning and memory, Nat. Rev. Neurosci. 23 (11) (2022) 666–682, https://doi.org/10.1038/s41583-022-00624-2.
[67] Q. Wang, M. Chen, N.P. Schafer, et al., Assemblies of calcium/calmodulin-dependent kinase II with actin and their dynamic regulation by calmodulin in dendritic spines, Proc. Natl. Acad. Sci. U.S.A. 116 (38) (2019) 18937–18942, https://doi.org/10.1073/pnas.1911452116.
[68] O. Shabtay, H. Breitbart, CaMKII prevents spontaneous acrosomal exocytosis in sperm through induction of actin polymerization, Dev. Biol. 415 (1) (2016) 64–74, https://doi.org/10.1016/j.ydbio.2016.05.008.
[69] M. Bosch, J. Castro, T. Saneyoshi, et al., Structural and molecular remodeling of dendritic spine substructures during long-term potentiation, Neuron 82 (2) (2014) 444–459, https://doi.org/10.1016/j.neuron.2014.03.021.
[70] M. Oser, J. Condeelis, The cofilin activity cycle in lamellipodia and invadopodia, J. Cell. Biochem. 108 (6) (2009) 1252–1262, https://doi.org/10.1002/jcb.22372.